Journal of Medicinal Chemistry

Article

Chemical Inhibition of Human Thymidylate Kinase and Structural Insights into the Phosphate Binding Loop and Ligand-induced Degradation

Yi-Hsuan Chen, Hua-Yi Hsu, Ming-Tyng Yeh, Chen-Cheng Chen, Chang-Yu Huang, Ying-Hsuan Chung, Zee-Fen Chang, Wei-Chen Kuo, Nei-li Chan, Jui-Hsia Weng, Bon-chu Chung, Yu-Ju Chen, Cheng-Bang Jian, Ching-Chieh Shen, Hwan-Ching Tai, Sheh-Yi Sheu, and Jim-Min Fang

J. Med. Chem., **Just Accepted Manuscript** • DOI: 10.1021/acs.jmedchem.6b01280 • Publication Date (Web): 17 Oct 2016

Just Accepted

ACS Publications

Journal of Medicinal Chemistry is published by the American Chemical Society. 1155 Sixteenth Street N.W., Washington, DC 20036

Chemical Inhibition of Human Thymidylate Kinase and Structural Insights into the Phosphate Binding Loop and Ligand-induced Degradation

Yi-Hsuan Chen,[1,§] Hua-Yi Hsu,[2,§] Ming-Tyng Yeh,[1] Chen-Cheng Chen,[3] Chang-Yu Huang[3], Ying-Hsuan Chung[3], Zee-Fen Chang,[3] Wei-Chen Kuo,[4] Nei-Li Chan,[4] Jui-Hsia Weng,[5] Bon-chu Chung,[5] Yu-Ju Chen,[1,6] Cheng-Bang Jian,[1] Ching-Chieh Shen,[1] Hwan-Ching Tai,[1] Sheh-Yi Sheu,[2,7,*] and Jim-Min Fang.[1,8,*]

[1] Department of Chemistry, National Taiwan University, Taipei 106, Taiwan.

[2] Department of Life Sciences and Institute of Genome Sciences, National Yang-Ming University, Taipei 112, Taiwan.

[3] Graduate Institute of Biochemistry and Molecular Biology, National Yang-Ming University, Taipei 112, Taiwan.

[4] Institute of Biochemistry and Molecular Biology, College of Medicine, National Taiwan University, Taipei 100, Taiwan.

[5] Institute of Molecular Biology, Academia Sinica, Taipei 115, Taiwan.

[6] Institute of Chemistry, Academia Sinica, Taipei, 115, Taiwan.

[7] Institute of Biomedical informatics, National Yang-Ming University, Taipei 112, Taiwan.

[8] The Genomics Research Center, Academia Sinica, Taipei 115, Taiwan.

§ Y.-H.C. and H.-Y.H. contributed equally to this work.

ABSTRACT

Targeting thymidylate kinase (TMPK) that catalyzes the phospho-transfer reaction for formation of dTDP from dTMP is a new strategy for anti-cancer treatment. This study is to understand the inhibitory mechanism of a previously identified human TMPK (hTMPK) inhibitor YMU1 (**1a**) by molecular docking, isothermal titration calorimetry, and photoaffinity labeling. The molecular dynamics simulation suggests that **1a** prefers binding at the catalytic site of hTMPK, whereas the hTMPK inhibitors that bear pyridino[*d*]isothiazolone or benzo[*d*]isothiazolone core structure in lieu of the dimethylpyridine-fused isothiazolone moiety in **1a** can have access to both the ATP-binding and catalytic sites. The binding sites of hTMPK inhibitors were validated by photoaffinity labeling and mass spectrometric studies. Taking together, **1a** and its analogues stabilize the conformation of ligand-induced degradation (LID) region of hTMPK and block the catalytic site or ATP-binding site, thus attenuating the ATP binding-induced closed conformation that is required for phosphorylation of dTMP.

Keywords:

Thymidylate kinase; Inhibitors; Molecular modeling; Photoaffinity probe; Isothermal titration calorimetry; Mass spectrometry.

INTRODUCTION

The enzymes of thymidylate synthesis have been targets for the actions of many anti-cancer drugs for more than 60 years.[1] However, human thymidylate kinase (TMPK, EC 2.7.4.9) has been a missing target, until our recent finding that blocking TMPK is able to sensitize cancer cells for low-dose doxorubicin chemotherapy.[2] Furthermore, the aggressive LKB-deficient lung cancers are hypersensitive to TMPK inhibition, suggesting the therapeutic applicability of TMPK inhibitors.[3] TMPK is a homodimeric enzyme that catalyzes the phosphorylation of dTMP to dTDP in the presence of Mg^{2+} ion and ATP.[4] According to the sequence and structure analyses,[5–7] the phosphate binding loop (P-loop), DR(Y/H) motif and ligand-induced degradation (LID) loop are highly conserved and essential for the function of TMPK.[8] P-loop binds the α- and β-phosphoryl groups of ATP. The Asp96 residue of DR(Y/H) motif binds the ATP–Mg^{2+} complex, while the Arg97 residue is involved in bringing ATP and dTMP together to induce a phosphoryl group transfer. The LID region is a flexible stretch nearby ATP binding site; however, its function in the connection of ATP (the phosphate donor) and dTMP (the phosphate acceptor) is unclear.[8]

The importance of TMPK in living organisms is attributed to its situated position at the junction of the de novo and salvage pathways of dTTP biosynthesis. TMPK is considered as a potential therapeutic target for various disease treatments.[9] For example, dTMP analogs have been synthesized as the inhibitors against the TMPK of *Mycobacterium tuberculosis*

(TMPKmt) to suppress *M. tuberculosis* infection.[10] Interestingly, these inhibitors have no inhibitory effect on human TMPK (hTMPK).[10] It is noted that the sequence variation surrounding the three essential loops confers inhibitor selectivity, even though the common folding structures of TMPK from different species are similar.[5, 11, 12]

We have previously shown that blocking hTMPK is able to sensitize cancer cells for low-dose doxorubicin chemotherapy, and identified YMU1 (**1a**) as a specific hTMPK inhibitor (Chart 1).[2] In contrast, **1a** has no inhibitory effect on the activity of purified thymidine kinase 1 (TK1) that is the enzyme responsible for the conversion of thymidine to dTMP.[2] The mechanistic investigation demonstrates that the lack of hTMPK functionality in cancer cells leads to dUTP misincorporation in DNA repair, resulting in cancer cell death. Overexpression of TMPK can rescue the DNA lesions caused by **1a**.[2] The conjunction treatment of **1a** with low dose of doxorubicin suppresses tumor growth in vitro and in vivo. Compound **1a** represents a new class of TMPK inhibitor since it is not a dTMP or nucleoside analog.[13] The kinetics study of TMPK revealed that **1a** is a mixed competitive inhibitor; however the detailed binding mode of **1a** has not yet resolved.[2] Understanding how **1a** inhibits hTMPK would provide useful information critical for optimization of hTMPK inhibitors.

Crystallographic analysis of the hTMPK–**1a** complex, either by co-crystallization or by soaking the pre-grown hTMPK crystals with **1a**, proved to be difficult. Thus, molecular

docking and probe labeling are two alternative approaches to study the binding sites of hTMPK. In this study, an ATP-free structure of hTMPK was used to perform molecular modeling experiments for understanding the molecular mechanism underlying hTMPK inhibition by **1a** and its arene-fused isothiazolone analogs **1b**–**3b** (Chart 1). A photoaffinity probe **4** bearing moieties of arylazide and biotin (Chart 1) was designed to identify the potential inhibitor binding sites of hTMPK.

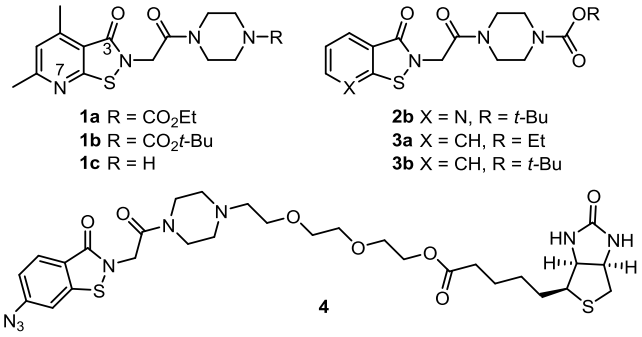

Chart 1. Chemical structures of **1a**, arene-fused isothiazolone analogues **1b**–**3b**, and photoaffinity probe **4**.

RESULTS AND DISCUSSION

The crystal structure of ATP-free form of hTMPK is constructed with the LID region for molecular simulations. Understanding the interaction of hTMPK with its inhibitors is critical for the development of pharmaceutical agents. Toward this aim, molecular simulations were performed to examine these interactions, and the important features for hTMPK–inhibitor recognition were described. We used the molecular mechanics/Poisson–

Boltzmann Surface Area method (MM/PBSA)[14] to estimate the enzyme–inhibitor binding affinity by looking at the free energy change of the system. We were unable to obtain diffracting crystals of hTMPK in complex with ligand, reflecting the fact that large structural rearrangements would be required to accommodate inhibitor access to the enzyme active site. Our kinetic analysis has shown that preincubation of **1a** reduces the ATP binding affinity of hTMPK;[2] therefore, the structure of an ATP-free form of hTMPK appears to be a more suitable starting point for structural modeling of hTMPK–inhibitor complexes. However, the LID region was not resolved in the crystal structure of ATP-free hTMPK, therefore we constructed the LID region based on the loop position in ADP-bound hTMPK (PDB 1E2D)[8] (Figure 1A). A comparison of the structures between the ATP-free and ADP-bound hTMPK was shown in Figure 1A; in ATP-free hTMPK, the modeled LID region was followed by 20 ns molecular dynamics (MD) simulation to obtain a relaxed conformation of the LID region (Figure 1C).

The analyses of the hydrogen-bonding network with the residues between the P-loop and the LID region are shown for the ADP-bound (Figure 1B) and the ATP-free hTMPKs followed by MD simulation (Figure 1D). This analysis points to the existence of a hydrogen-bonding network within the ATP binding site, consisting of residues Asp15, Arg16, Ala17, Arg143, Gly144, Glu152, and Ala180 (Figure 1B); the ATP binds in a cleft lined by Arg16, Gly18, Lys19, Ser20, Thr21, Arg143, and Lys182. A distinct conformation between

ADP-bound and ATP-free forms is the P-loop. In ADP-bound form, Arg16 points to the LID region and forms hydrogen-bonds with Gly144, Ala145, and Glu152; the carboxyl group of Asp15 and the phosphate groups of ADP and TMP coordinates with Mg^{2+} (Figure 1B). In ATP-free form, the residues of Asp15, Arg16, Ala17, and Glu149 form hydrogen-bonding network; the side chain of Arg16 points to the phosphate group of TMP and the carboxyl groups of Asp15 and Glu152 chelate Mg^{2+} ion (Figure 1D). Due to the loss of the ATP interaction, the LID region becomes more flexible after MD simulation.

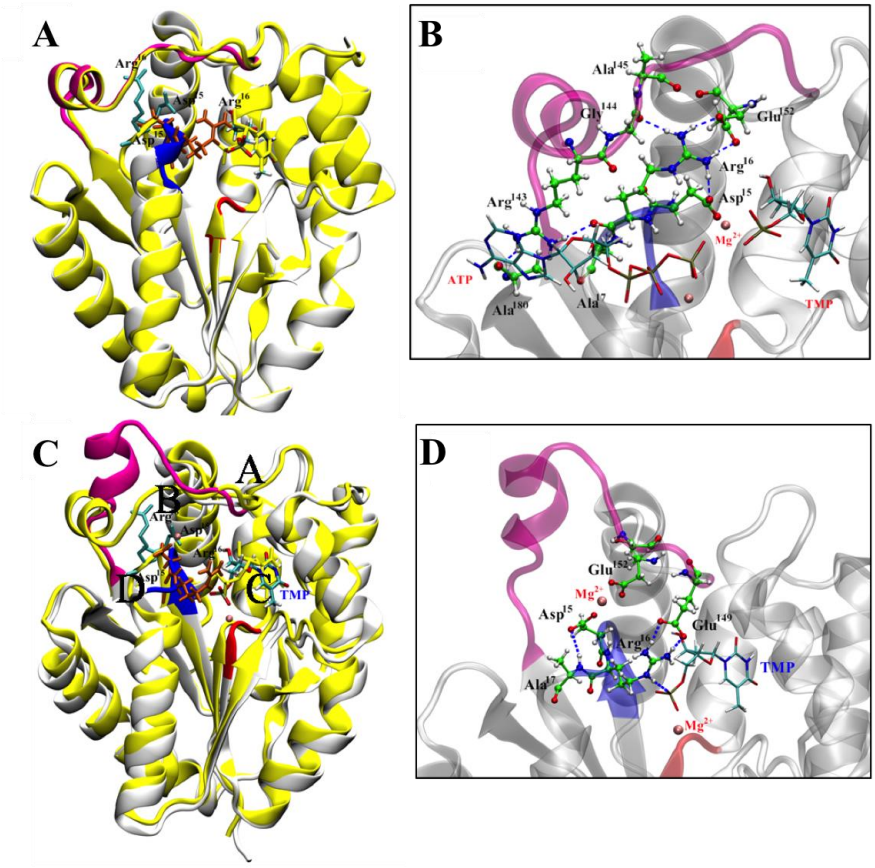

Figure 1. Structural model of hTMPK. (A) Overlap of the structures of ADP-bound hTMPK (yellow) and the ATP-free hTMPK (gray). Residues of the P-loop (13–17) are shown in ball

and stick representation and colored in blue; the LID region (135–150) can be seen in magenta; the DR motif (Asp96/Arg97) is shown in red. (B) Close-up view of the ADP binding site with residues shown. TMP is shown in stick representation with its color based on atom type, carbon (green), oxygen (red), nitrogen (blue) and hydrogen (white); Mg^{2+} ion is shown in pink. The hydrogen-bonds are shown in dash lines. (C) Depiction of the structures of the relaxed ATP-free TMPK (gray) and the ADP-bound hTMPK (yellow). Four possible ligand docking sites are denoted as A, B, C and D sites, which were created using AutoDock Vina program[15]. (D) Close-up view of ATP-free hTMPK structure with relaxed LID region and residues shown.

Molecular docking analysis with 1a reveals four binding sites in hTMPK. We then performed the docking analysis with compound **1a** to screen possible binding sites. The results revealed four related binding sites for **1a** in Figure 1C, where A-site is above the LID region, B-site is surrounding the catalytic pocket between P-loop and LID region, C-site is beneath and surrounding TMP, and D-site is ATP binding site. When both ATP and dTMP exist, an ATP molecule will reside at the D-site and a dTMP molecule will reside at the C-site. During the phospho-transfer process, the ATP molecule will be relocated from D-site to the catalytic pocket (B-site) to furnish the phosphorylation reaction of dTMP.[8] The docking scores show that A- and C-sites are not good for ligand binding, while B- and D-sites have higher

docking scores. Therefore, both B- and D-sites are used to investigate the inhibitory mechanism at the molecular level.

In the catalytic pocket (B-site), the optimized structure of the hTMPK–**1a** complex subjected to 35 ns MD simulation is shown (Figure 2A). Structural properties were monitored by computing the root-mean-square deviation (RMSD) between the snapshots during the MD simulation and the starting coordinates to ascertain that the simulations were stable and converged. The RMSD computed for the complex hTMPK–**1a** backbone atoms was very stable with the value below 2.5 Å (Figure S1A in Supporting Information (SI)). The residues Ala141, Ala145, Phe146, Ala140, Leu137, Leu135, Ala17, and Val14 form a hydrophobic pocket surrounding compound **1a**. We found that the flexibility of the LID region is dramatic in the ligand-free hTMPK. In contrast, in the hTMPK–**1a** complex, **1a** interacts with LID region and forms hydrogen-bonds with the amide N atoms of Ala145 and Glu149 to slow down the motion of LID region (Figure S1B and S1C in SI). Therefore, the molecular mechanism of **1a** in inhibition of hTMPK is considered to disrupt the hydrogen-bonding network between LID region and P-loop and blocks the catalytic site, after which ATP binding is unable to induce a closed conformation required for the catalytic reaction of hTMPK.

Molecular docking analyses predict compounds 2b and 3b are able to bind at either the ATP-binding or catalytic sites of hTMPK. According to our hTMPK inhibition assays,

compounds **1a**, **1b** and **1c** that bear the end groups (CO_2Et, CO_2*t*-Bu and H) in different sizes did not have appreciable effect on the inhibitory activity. According to data of **1a** with hTMPK, we thus undertook the molecular docking analyses of compounds **2b** and **3b** to compare their binding modes with that of **1a** in hTMPK. Instead of the ethoxycarbonyl group in **1a**, both **2b** and **3b** have a bulkier *tert*-butoxycarbonyl (Boc) group at the end. Compound **2b** modifies the dimethylpyridine-fused isothiazolone moiety in **1b** by deletion of the two methyl substituents, whereas **3b** further changes the core structure to benzo[*d*]isothiazolone. The binding modes of **1a**, **2b** and **3b** to hTMPK are shown in Figure 2A–F. The binding free energies of three ligands and the assay results are listed in Figure 2G, while the detailed energy components are given in SI (Table S1).

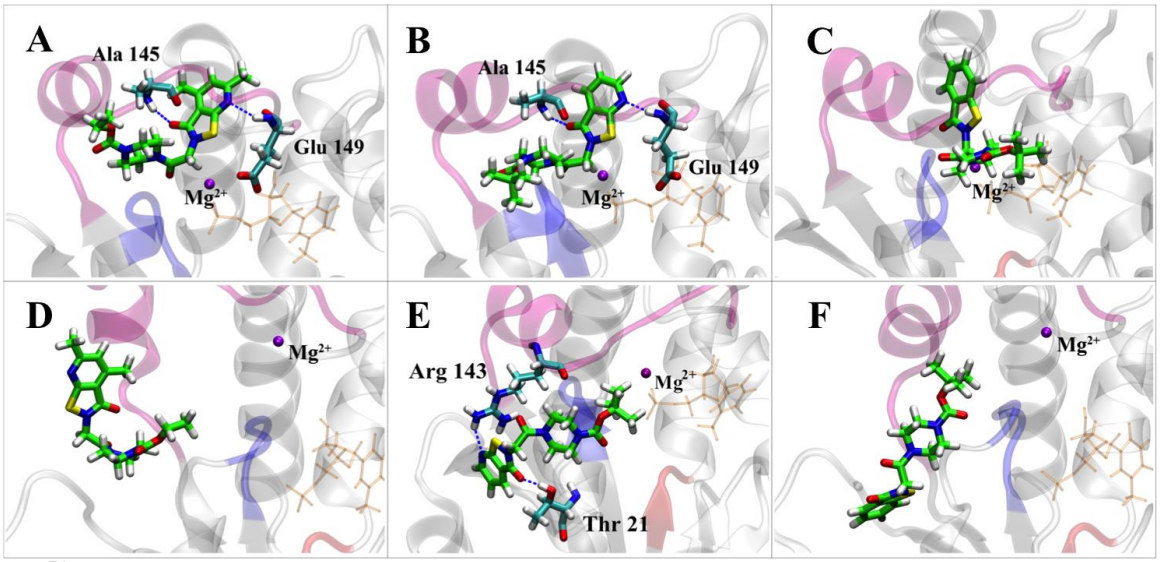

G

ligand		**1a** (YMU1)	**2b**	**3b**
$\Delta G_{binding}$ (kcal/mol)[a, b]	B-site	–39.8 ± 0.6	–23.3 ± 0.2	–16.2 ± 0.2
	D-site	N.D.[c]	–21.1 ± 0.6	–18.6 ± 0.3
IC_{50} (μM)[a, d]		1.65 ± 1.10	0.47 ± 0.08	0.35 ± 0.01
EC_{50} (μM) [a, e]		0.88 ± 0.30	1.40 ± 0.50	0.65 ± 0.04

Figure 2. Binding modes of hTMPK–ligand complexes and the assay results. (A) compound **1a** in the catalytic site, (B) compound **2b** in the catalytic site, (C) compound **3b** in the catalytic site, (D) compound **1a** in the ATP-binding site, (E) compound **2b** in the ATP-binding site, and (F) compound **3b** in the ATP-binding site. All notations are the same as the legend of Figure 1. Hydrogen bond is shown in blue (dash line). The structure was taken from the last 35 ns MD trajectory. (G) Ligand binding free energy ($\Delta G_{binding}$), IC_{50} and EC_{50} values against hTMPK. [a] Errors are given as standard deviation (SD). [b] Ligand binding free energies are calculated according to Eq. [1] (see Experimental section). [c] N.D.: not detected. [d] IC_{50}values are derived from luciferase-coupled TMPK assay in triplicate independent experiments. [e] EC_{50} vales are derived from viability assay of 32D/Bcr-Abl cancer cells in triplicate independent experiments.

The binding mode of **2b** at the catalytic site (Figure 2B) is similar to that of **1a** (Figure 2A), stabilizing Ala145 and Glu149 through hydrogen bonding with the C_3 carbonyl and the N_7 atom of the heterocyclic core structure. However, the binding free energy ($\Delta G_{binding}$ = –23.3 kcal/mol) of **2b** at the B-site is still weaker than that of **1a** ($\Delta G_{binding}$ = –39.8 kcal/mol) (Figure 2G). When **3b** was superimposed into the catalytic site (B-site) based on the position of **1a**, there is no hydrogen bond between hTMPK and **3b**, thus the binding free energy is further decreased ($\Delta G_{binding}$ = –16.2 kcal/mol). These results indicate that the pyridine moiety of **1a** and **2b** may be superior to the benzene moiety of **3b** to exert hydrogen bonds for better binding affinity in the B-site of TMPK.

In sharp contrast, the MD simulation shows that **1a** is unable to reside at the ATP-binding site (D-site), presumably because the methyl groups of the heterocyclic core would cause severe hindrance (Figure 2D). In comparison, **2b** can form hydrogen bonds via N_7····HN(Arg143) and O_3····HO_β(Thr21) at the D-site (Figure 2E). Compound **3b** also prefers to stay at the D-site during MD simulation through hydrophobic interactions (Figure 3F). Taken together the MD simulations at B- and D-sites, a ligand (e.g. **2b** and **3b**) capable of blocking both sites may become a stronger TMPK inhibitor than **1a** that only adapts a single B-site. This deduction is supported by measurement of the inhibitory activity against hTMPK (Figure 2G).

Synthesis of compounds for evaluation of hTMPK inhibitory activity. To verify the binding affinity predicted by the MD simulation, compounds **1a**–**3b** were synthesized and the inhibitory activities against hTMPK were measured (Figure 2G). The synthesis of compound **1a** has been reported,[2] and the analogous compounds **1b**, **2b** and **3b** were synthesized by the similar procedures (Scheme 1). For example, 2-chloronicotinonitrile was reacted with thiourea to give 2-mercaptonicotinonitrile (**5b**),[20] which was then treated in concentrated H_2SO_4 to give pyridine-fused isothiazolone **6b** as the oxidative cyclization product.[2] The reaction of **6b** with a relatively soft electrophile of iodine reagent **7** afforded the *N*-alkylation product **2b**, predominating over the *O*-alkylation. Compound **1c** was obtained by removing the Boc group in **1b** with trifluoroacetic acid (TFA).

Scheme 1. Synthesis of hTMPK inhibitors **1b**–**3b**.

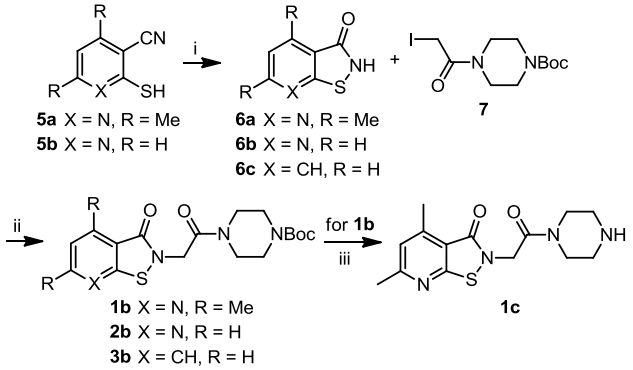

Reagents and conditions: (i) conc. H_2SO_4, reflux, 4–5 h; **6a**, 61%; **6b**, 30%. (ii) Cs_2CO_3, Et_3N, CH_2Cl_2, rt, 5–24 h; **1b**, 59%; **2b**, 40%; **3b**, 60%. (iii) TFA, CH_2Cl_2, rt, 0.5 h; 100%.

Photoaffinity labeling provides a directly way to identify the binding domain within the target protein.[16] To design a photoaffinity probe, structural modification of pharmaceutical skeleton is needed by incorporation of photosensitive group and reporter unit.[17] We chose aryl azide as the photoreactive group[18] and a biotin tag to merge with the structural skeleton of the potent compound **3b**. Thus, the photoaffinity probe **4** was constructed to identify the interactions between hTMPK and this new class of inhibitors. Furthermore, purification of the covalently bound hTMPK–**4** complex would be facilitated by the biotin tag.[19] Scheme 2 shows the synthesis of probe **4**. The substitution reaction of 4-bromo-2-fluorobenzonitrile with Na_2S occurred selectively via an addition–elimination mechanism to give 4-bromo-2-mercaptobenzonitrile (**5d**),[20] which underwent an oxidative cyclization reaction in concentrated H_2SO_4 to give benzoisothiazolone **6d**.[2] The *N*-alkylation of **6d** with iodine reagent **7** was carried out to afford **8**. The reaction of aryl bromide **8** with NaN_3 in the presence of CuI, sodium ascorbate and *N*,*N*′-dimethylethylenediamine (DMEDA) gave the desired azido product **10**, albeit in low yield (12%).[21] The major product turned out to be the aniline **9** (58%), though the mechanism for its formation was unclear. It has been suggested that azidobenzene may undergo in situ reduction to aniline in the reaction conditions containing CuI and NaN_3.[22] Fortunately, aniline **9** could be treated with $NaNO_2$ and NaN_3 in acidic condition to give the desired azido compound **10**, presumably via Sandmeyer reaction of the intermediate diazonium salt.[23] The Boc protecting group in **10** was removed by TFA to

give amine **11**, which was then linked to a biotin labeling reagent **12** to furnish the photoaffinity probe **4**.[24]

Scheme 2. Synthesis of probe **4**.

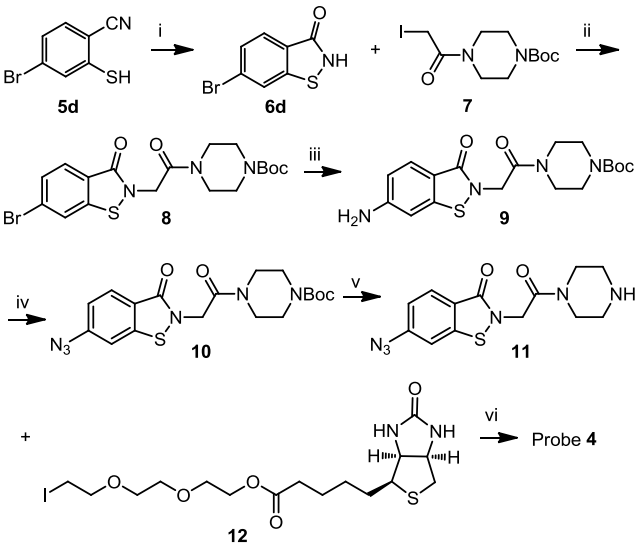

Reagents and conditions: (i) conc. H_2SO_4, reflux, 5 h; 94%. (ii) *i*-Pr_2NEt, THF, rt, 4 h; 41%. (iii) NaN_3, sodium ascorbate, CuI, DMEDA, EtOH, H_2O, 100 ^oC, 2 h; 58%. (iv) $NaNO_2$, NaN_3, *N*-methyl-2-pyrrolidonium bisulfate, H_2O, 1 h; 45%. (v) CF_3CO_2H, CH_2Cl_2, 30 min; 87%. (vi) Et_3N, DMSO, 8 h; 40%. DMEDA is *N*,*N*′-dimethylethylenediamine.

hTMPK inhibition assay supports that compounds 2b and 3b are stronger inhibitors than 1a. A luciferase-coupled TMPK assay[25] was applied to evaluate the inhibitory activity of **1a**–**4** against hTMPK. Our previous study has indicated that compound **1a** is an effective inhibitor against hTMPK, showing 70.0 ± 7.0% inhibition at a

concentration of 2 μM. Compounds **1b** and **1c** at 2 μM also showed similar inhibitory activities (76.3 ± 2.5% and 73.4 ± 5.7%) regardless the change of end R groups (CO_2Et in **1a**, CO_2*t*-Bu in **1b** and H in **1c**). In comparison, change of the heterocyclic core structure caused remarkable effect as shown by much stronger hTMPK inhibition of compounds **2b** and **3b** (91.3 ± 4.0% and 91.3 ± 5.7% at 2 μM). Probe **4** at 2 μM inhibited 86.9 ± 0.7% of hTMPK activity, indicating that the small azido substituent and the long-chain end group did not interfere with the binding in hTMPK. The IC_{50} values of **1a**, **2b** and **3b** were determined to be 1.65 ± 1.1, 0.47 ± 0.08 and 0.35 ± 0.01 μM by luciferase-coupled TMPK assay, respectively (Figure 2G), indicating that **2b** and **3b** are stronger binders than **1a**. The conventional NADH-coupled assay also confirmed that compounds **2b** and **3b** had higher hTMPK inhibitory activity than **1a** (Figure S2 in SI). As suggested by the MD simulations (Figure 2), a compound can bind at either the B- or D-site to suppress the activity of hTMPK. In comparison, **1a** can only have access to B-site, while compounds **2b** and **3b** can be incorporated into both the B- and D-sites of hTMPK. The higher inhibitory activity of **2a** and **3b** may be related to the higher probability of access to hTMPK.

The ability of these compounds on suppressing viability in normal versus cancer cells was further compared. To this end, we chose 32D myeloid progenitor cells as normal and Bcr-Abl transformed 32D as cancer cells. Bcr-Abl is a hallmark of chronic myeloid leukemia due to chromosomal reciprocal translocation between chromosome 22 and chromosome 9

(t(9;22)(q34;q11)). The resulting Bcr-Abl fusion protein transforms normal hematopoietic cells into leukemic cells[26]. We treated 32D and 32D/Bcr-Abl- cells with **1a**, **2b** and **3b** for viability determination. Treatment with compounds **1a**, **2b** and **3b** up to 2 μM for 3 days did not cause appreciable effect on 32D cells (Figure S3 in SI). In contrast, **1a**, **2b** and **3b** were toxic to 32D/Bcr-Abl cells, showing EC_{50} values of 0.88, 1.40 and 0.65 μM, respectively (Figure 2G). Compared to **1a** and **2b**, the benzo[*d*]isothiazolone **3b** was more effective and selective in inhibiting cell proliferating in Bcr-Abl transformed leukemia cells.

Isothermal titration calorimetry reveals that the hTMPK–inhibitor complex is formed in 1:1 stoichiometry. Isothermal titration calorimetry (ITC) was performed to elucidate the binding mode of inhibitor with hTMPK. In ITC experiment, it is necessary to have the test compound and protein solubilized in the same solution. Both compound **1c** (containing an amine moiety) and hTMPK are soluble in PBS buffer (pH = 7.4), and thus suitable for the ITC experiment. In contrast, compounds **2b** and **3b** cannot dissolve well in PBS buffer without addition of DMSO. As compound **1c** still has an appreciable inhibitory activity against hTMPK, we thus chose **1c** to perform the ITC analysis (Figure 3). The ITC experiment confirms that **1c** binds with hTMPK to form an hTMPK–**1c** complex in 1:1 stoichiometry with the binding constant of 127,000 ± 19,600 M^{-1} in PBS solution. The disposition of compound **1c** in the active site of hTMPK is thermodynamically favored as

shown by the negative free-energy change that is mainly attributed to the enthalpy change (ΔH = –6.95 kcal/mol) with very little entropy change (ΔS = 0.047 cal/mol/deg).

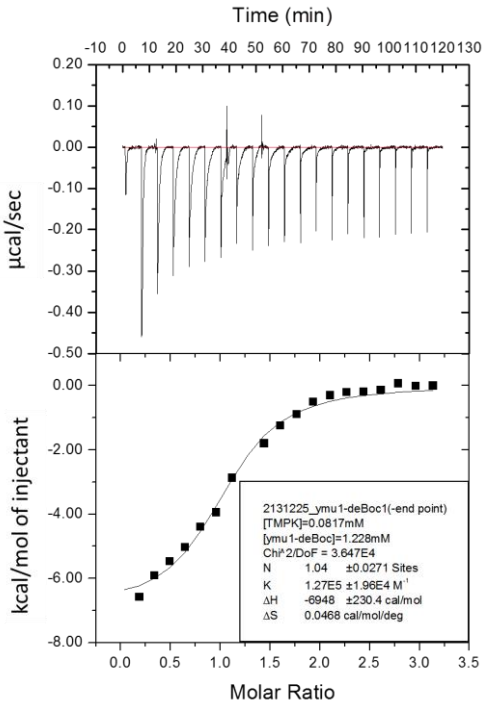

Figure 3. Isothermal titration calorimetry (ITC) experiment. ITC shows that hTMPK and compound **1c** forms a complex of 1:1 stoichiometry in PBS solution.

Amino acid residues in proximity of the ATP-binding site of hTMPK are identified by photoaffinity labeling and mass spectrometric analysis. Probe **4** containing a photoreactive arylazide moiety and a biotin affinity handle was preincubated with purified hTMPK protein in PBS buffer at 25 ^{o}C for 30 min, and then subjected to irradiation with 254-nm UV light (Figure 4A).[27] The highly reactive nitrene intermediate was expected to cross link with hTMPK by forming covalent bonds with the proximate amino acid residues in

the active site.[18] The covalent attachment of probe **4** to hTMPK was visualized by streptavidin–horseradish peroxidase (HRP) in Western blot analysis (Figure 4B). The photolabeling experiment was also carried out without preincubation. In the absence of UV light, we did not observe non-specific labeling of hTMPK (Figure 4B).

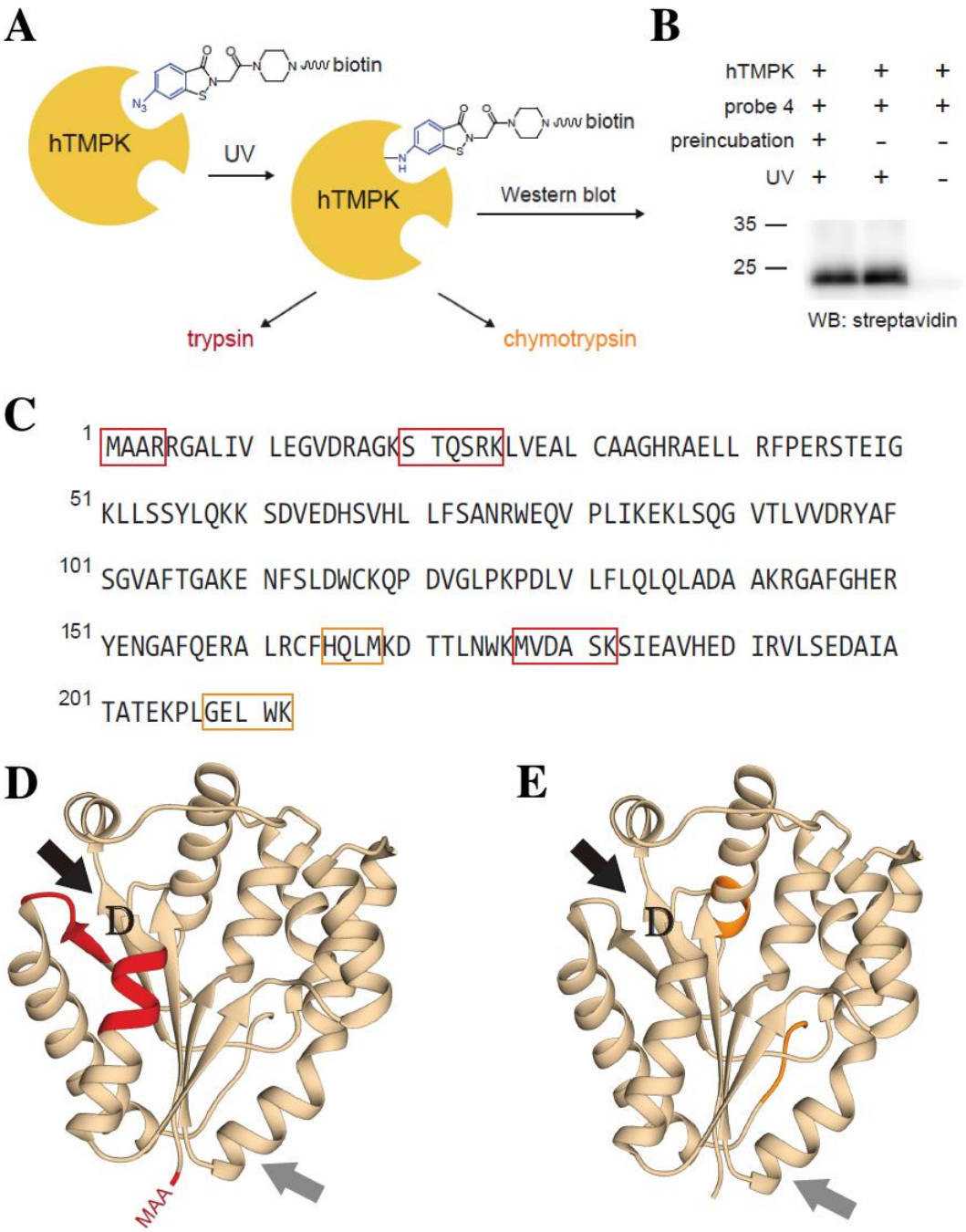

Figure 4. Photoaffinity probe labeling. (A) Schematic for photoaffinity labeling. (B) Western blot of hTMPK photolabeled with probe **4**, visualized using streptavidin–horseradish peroxidase. (C) Sequences of photolabeled peptides. Photolabeled hTMPK was separately digested with trypsin and chymotrypsin, and biotinylated peptides were enriched by affinity

chromatography and analyzed by LC–MS/MS. Tryptic and chymotryptic peptides showing probe conjugation are marked by red and orange boxes, respectively. (D) & (E) Positions of photolabeled peptides mapped to hTMPK structure (PDB: 1E2D, no coordinates available for N-terminal residues MAA), with tryptic peptides marked in red (D) and chymotryptic peptide in orange (E). The D-site is marked, and the black and grey arrows indicate two general binding regions of the probe **4**.

The modification sites of hTMPK by probe **4** were investigated by a mass spectrometric approach. We utilized two different proteases, trypsin and chymotrypsin, to separately digest photolabeled hTMPK. By affinity chromatography with immobilized monomeric avidin, the photolabeled peptides bearing terminal biotin moiety were enriched and then subjected to LC–MS/MS analysis (Figure 4C). The ester linkage in probe **4** was sometimes hydrolyzed under the acidic condition of reversed-phase chromatography, and hence the mass shift of labeled peptides was either +648.24 or +422.16 Da (Table S2 in SI). We used both mass shift and strong enrichment during avidin affinity chromatography as the criteria for identification of modified peptides. With trypsin and chymotrypsin digestion, we identified three and two probe-modified peptides, respectively (Figure 4C and Table S2). By mapping these three modified peptides onto the three dimensional structure of hTMPK, two tryptic (residues 20–25 and 177–182, Table S2) and one chymotryptic peptide (165–168) appeared at or in the

vicinity of D-site (indicated by black arrow in Figures 4D and 4E). The extreme N-terminus and the extreme C-terminus, which were unstructured in crystallography and in close proximity, were also labeled by probe **4**. This probably represented a nonspecific binding site on the opposite face of the catalytic pocket (indicated by grey arrow in Figures 4D and 4E). Combining the results of trypsin and chymotrypsin digestion, the primary binding sites of probe **4** appeared to be the ATP binding site (D-site), consistent with the molecular docking results of compound **3b** (Figure 2), from which probe **4** was derived. Though no probe-modified peptides for binding of probe **4** at the B-site were found in our experiment, one should not overlook the possibility that our current experiment might not be sensitive enough to detect such probe-modified peptides that could occur in small amount or difficult to ionization in MS analysis.

TMPK inhibitors 1a–4 are not PAINS. There is a concern about whether compounds **1a**–**4** are pan assay interference compounds (PAINS).[28,29] Multiple lines of experimental evidence exclude this possibility. (1) Our previous work[2] has revealed that **1a** has no inhibitory effect on the activity of purified thymidine kinase 1 (TK1) that is the enzyme responsible for the conversion of thymidine to dTMP. (2) We also demonstrates that the effect of **1a** on impairing DNA repair can be suppressed by three different molecular events that can remove dUTP misincorporation in DNA.[2] These molecular events include overexpression of

dUTPase, knockdown of uracil-DNA glycosylase and disruption of ribonucleotide reductase recruitment to DNA damage sites. If **1a** were a PAIN, the effect of **1a** would not have been overcome by these events. (3) In this study, we further show that **1a** and its analogs (**2b**, **3b** and **4**) have no inhibitory effect on tyrosine kinase activity (IC_{50} > 100 μM) (Table S3 in SI). (4) The TLC monitored isotope labeling experiment shows that **1a** inhibits the formation of ^{32}P-dTDP by human TMPK but not candida Cdc8, which is a human TMPK ortholog sharing 41% identity in amino-acid sequence (Figure S4 in SI). (5) Normal cells (e.g. 32D myeloid progenitor cells) are not affected by treatment of **1a** at 2 μM for 3 days (Figure S3 in SI), suggesting no appreciable toxicity of **1a**. If **1a** had nonspecific inhibitory effect, the growth of normal cells would have been affected. (6) Promiscuous PAINS often contain the functional groups (e.g., alkyl halide and α,β-unsaturated ester) that are reactive to the nucleophilic sulfanyl group of Cys residue. However, no protein band corresponding to nonspecific addition of Cys is observed in Western blot after incubation of probe **4** with hTMPK under UV-free condition (Figure 4B). (7) The three Cys residues (Cys31, Cys117 and Cys163) in hTMPK are mapped (Figure S5 in SI), but none of them exist in the ATP-binding site or catalytic site. Although Cys163 is in the proximity of hTMPK active site, irradiation of probe **4** labels its neighboring region (165–168) but not this particular residue (Figure 4C). (8) 2-Phenylbenzo[*d*]isothiazol-3(2*H*)-one (structure **A** in Chart S1 of SI) is considered a PAIN acting as a covalent modifier of proteins.[29] We thus examined whether compounds **1a** and **A**

could be attacked by the Cys residues of hTMPK? We chose Ellman′s reagent, 5,5′-dithiobis(2-nitrobenzoic acid) (DTNB), as a positive control and DMSO vehicle as a negative control. After incubation of hTMPK with **1a**, **A** and DTNB at 25 ^{o}C for 30 min, respectively, the hTMPK solutions were readily digested by trypsin, without prior reduction with dithiothreitol (DTT). The LC–MS/MS analyses showed 95–100% coverage of the hTMPK sequence, and only compounds **A** and DTNB modified hTMPK by formation of disulfide bonds with Cys residues (Table S4 in SI). This result confirms that the binding of **1a** with hTMPK is noncovalent and not through disulfide formation. Taking together the evidence from different enzymatic and cell-based assays, compounds **1a**–**4** are specific hTMPK inhibitors, and unlikely belong to the category of PAINS.

We also found that benzoisothiazolone compounds bearing different substituents may alter their binding modes. For comparison, we prepared compounds **13**–**17** (Chart S1 in SI) having the structures related to the hTMPK inhibitors **1a**–**3b**. Their inhibitory activities were evaluated by luciferase-coupled TMPK assay. Though compound **3a** is an effective hTMPK inhibitor (70% inhibition at 2 μM), compound **13** that is structurally similar to **3a** but having a longer linker showed no appreciable hTMPK inhibitory activity (7% inhibition at 2 μM). Unlike PAIN compound **A**, benzoisothiazolone **14** having a 3-chloro-4-fluorophenyl substituent, instead of the phenyl group in **A**, did not bind with hTMPK (< 2% inhibition at 2 μM). Unlike **1a**, **2b** and **3b** that were derived from *N*-alkylation, the corresponding

O-alkylation compounds **15**–**17** showed low hTMPK inhibition. It is clear that not all benzoisothiazole or pyridinoisothiazole compounds are PAINS.

CONCLUSIONS

TMPK is situated at the pivotal position of the de novo and salvage pathways of dTTP biosynthesis. When the functionality of TMPK is suppressed, the supply of dTTP is reduced, and dUTP misincorporation can occur in DNA repair to cause cancer cell death. Compound **1a** is a specific hTMPK inhibitor to sensitize cancer cells for low-dose doxorubicin chemotherapy.[2] Compound **1a** contains the main structural scaffold of pyridine-fused isothiazolone that belongs to a new class of TMPK inhibitor. To understand the binding mode of **1a** in hTMPK will help to develop this new class of hTMPK inhibitors in cancer treatment.

In this study, we first carry out molecular simulations using the crystal structure of an ATP-free form of hTMPK with implantation of the LID region to show the important features and interactions of hTMPK with the arene-fused isothiazolone inhibitors. According to the results of our molecular docking experiments, hTMPK has an ATP binding site (D-site) and a B-site surrounding the catalytic pocket between P-loop and LID region to incorporate the arene-fused isothiazolone inhibitors. The ITC analysis confirms that the arene-fused isothiazolone inhibitor forms a 1:1 complex with hTMPK. Compound **1a** prefers to bind at the B-site of hTMPK, whereas compounds **2b** and **3b** can bind at ether the B- or D-sites.

Thus, compounds **2b** (IC_{50} = 0.47 μM) and **3b** (IC_{50} = 0.35 μM) exhibit about 4-fold higher binding affinity than **1a** (IC_{50} = 1.65 μM). In the cell viability assay, compound **3b** inhibits the proliferation of Bcr-Abl transformed 32D cell with more efficiency but less cytotoxicity to 32D myeloid progenitor cells compared to compound **1a**.

As the end groups in these compounds do not exhibit appreciable effect on the hTMPK inhibitory activity, the photoaffinity probe **4** is designed to bear a photoreactive moiety of arylazide and a biotin tag. The photoaffinity labeling experiment works well to tag the interacting amino acid residues in the active sites of hTMPK. The probe-modified peptides are identified by mass spectrometric method to show that most of the interacting peptides occur at the D-site as predicted by our molecular docking experiments. The preferable location of compounds **2b**, **3b** and **4** in the ATP-binding site may be attributable to their main structures of pyridine- and benzene-fused isothiazolones that act as proper mimetics of the purine moiety of ATP. In comparison, **1a** has less inhibitory activity presumably because it has two methyl groups on the pyridine ring to make severe hindrance against its disposition in the ATP-binding site. Taking together, our present study provides clear evidence for the binding mode of the arene-fused isothiazolone inhibitors, which disrupt the connection between LID region and P-loop that are crucial to the function of hTMPK in phospho-transfer from ATP to dTMP. As TMPK inhibition can selectively sensitize cancer cells to low-dose

chemotherapy, the structural information of TMPK–inhibitor will be useful for design of potent inhibitors in various cancer treatments.

EXPERIMENTAL SECTION

General. All the reagents and solvents were commercially available and used without further purification unless indicated otherwise. All solvents were anhydrous grade unless indicated otherwise. Dichloromethane (CH_2Cl_2) was distilled from CaH_2. All air or moisture sensitive experiments were performed under nitrogen. Reactions were magnetically stirred and monitored by thin-layer chromatography (TLC) on 0.25 mm E. Merck silica gel 60 F_{254} glass plates. Compounds were visualized by UV, or using *p*-anisaldehyde, ninhydrin and phosphomolybdic acid (PMA) as visualizing agent. E. Merck silica gel 60 (0.040–0.063 mm particle sizes) was used for flash chromatography.

Instrumentation. Melting points were recorded on a Yanaco melting point apparatus. Optical rotations were measured on a digital polarimeter of Japan JASCO Co. DIP-1000. $[\alpha]_D$ values are given in units of 10^{-1} deg cm^2 g^{-1}. Infrared (IR) spectra were recorded on Thermo Scientific Nicolet iS5 FT-IR spectrometer. UV–Vis spectra were measured on PerkinElmer Lamda 35 UV–Vis spectrometer. Nuclear magnetic resonance (NMR) spectra were obtained on Varian Unity Plus-400 (400 MHz) spectrometer, and chemical shifts (δ) were recorded in parts per million (ppm) relative to internal standards: $CHCl_3$ (δ_H = 7.24), $CDCl_3$ (δ_C = 77.0

for the central line of triplet), CH_3OD (δ_H = 3.31), CD_3OD (δ_C = 49.0), $(CH_3)_2SO$ (δ_H = 2.50) and $(CD_3)_2SO$ (δ_C = 39.5). The splitting patterns are reported as s (singlet), d (doublet), t (triplet), q (quartet), m (multiplet), br (broad) and dd (doublet of doublets). Coupling constants (*J*) are given in hertz (Hz). ESI–HRMS spectra were recorded on a Bruker Daltonics BioTOF III high-resolution mass spectrometer. LC–MS/MS was conducted on Waters ACQUITY nanoUPLC system conjugated with Waters Synapt G2 HDMS (Milford, MA, USA). High-performance liquid chromatography (HPLC) was performed on Agilent 1100 Series instrument equipped with a degasser, Quat pump and UV detector.

Protein and ligand setup. The missing LID region in ATP-free hTMPK structure was modeled based on the template (Protein Data Bank entry 1E2D).[8] Solvent molecules were removed, retaining TMP and Mg^{2+} ions. All hydrogen atoms were added, and then the protein structure was subjected to energy minimization using the NAMD program[30] with the CHARMM27 force field.[31] The optimized structures and partial charges for the ligands were obtained using the Gaussian 09 program with the 6-31G(d,p) basis set.[32]

Docking. All docking runs were performed with version 1.1.2 of the AutoDock Vina program.[15] MGL Tools were used to generate the structure format (PDBQT) for Autodock Vina, and nonpolar hydrogens were removed. First, in order to screen for the best binding sites, the ligand was docked against TMPK with a large grid box 50 × 50 × 50 $Å^3$ to include the ligand and protein for a global search. Mg^{2+} ions were removed. Protein was fixed and the single bonds of ligands were flexible during the process. This approach obtains an evaluation of scoring function during the docking process, so that as many conformations as possible can be detected. The minimum scoring value indicates the most likely conformation. We compared and selected the binding sites and docking affinities that have the highest ranking

scores, corresponding to the non-bonded van der Waals and electrostatic interactions between ligand and protein in the implicit water system. Thus, the grid box was centered on the ligand in its binding mode with a smaller box size 36 × 26 × 26 $Å^3$ for a local search. A grid spacing of 1 Å was used, and the grid size was large to extend at least 6 Å beyond any ligand atom in its binding mode. Flexible torsions were defined with torsion tree/choose torsion. The docking process consisted of 5 independent runs per ligand and 9 binding modes were generated. The results were represented with the best binding affinity.

Based on these results, Mg^{2+} ions were added to the protein–ligand complex model in their crystallographic positions, and nonpolar hydrogen atoms were generated. The complex structure was subjected to energy minimization with a harmonic constrained force of 100 (kcal/mol $Å^2$) on the backbone atoms, then on the Cα atoms, followed by gradually removing the constraints. A further 1×10^5 steps of minimization were performed to obtain an optimal structure, followed by MD simulations.

Computational procedures and binding free energy calculation. Molecular dynamics (MD) simulations were performed by the NAMD program[30] with the CHARMM27 force field[31] to study the interactions of the ligands binding to hTMPK. The minimized hTMPK–ligand complex was solvated with TIP3P[33] water molecules in a 70 × 70 × 70 $Å^3$ cubic box with 150 mM NaCl ionic strength. A periodic boundary condition and Particle Mesh Ewald (PME) algorithm[34] were applied, and the non-bonding cutoff was set at 14 Å. The simulation was carried out under the temperature and pressure at 300 K and 1 atm. The system was subjected to 2 ns MD simulation to equilibration, followed by 30 ns of production simulation. All molecular visualizations and graphics were carried out using the VMD program.[35]

The binding free energy between hTMPK and ligand was computed by using the molecular mechanics Poisson–Boltzmann surface area (MM/PBSA) method[36]. The binding free energy $\Delta G_{binding}$ is calculated according to Eq. [1]:

$$\Delta G_{binding} = \Delta G_{ligand-enz} - (\Delta G_{ligand} + \Delta G_{enz}) \quad [1]$$

If ΔG_X represents the free energy of species X, it can be calculated from Eq. [2]:

$$\Delta G_X = E_{MM} + \Delta G_{solv} - T\Delta S) \quad [2]$$

E_{MM} is the molecular mechanical energy obtained from the equation:

$$E_{MM} = E_{internal} + E_{vdW} + E_{elect} \quad [3]$$

Where $E_{internal}$, E_{vdW} and E_{elect} are the internal energy of the molecule, the non-bonded interaction energy from the van der Waals interaction, and electrostatic interaction, respectively. The solvation free energy ΔG_{solv} represents the polar free energy (ΔG_{polar}) and the nonpolar free energy ($\Delta G_{nonpolar}$) of solvation; the polar part is calculated by the APBS program[36] and the nonpolar part is calculated from the equation:

$$\Delta G_{nonpolar} = \beta + \gamma \times \Delta A \quad [4]$$

In Eq. [4], ΔA is the solvent accessible surface area change of the molecule, the parameter β is 0.92 kcal/mol, and γ is 0.00542 kcal/mol Å ^{2}.[14] For the solute entropic contribution to the system ($T\Delta S$), ΔS is calculated by normal mode analysis and T is temperature in K.

Plasmids, expression and purification of enzymes. Human TMPK cloned in pGEX-2T was transformed in *E. coli* JM109 strain to produce GST-hTMPK fusion protein, which was

purified by glutathione 4B beads (Amersham Pharmacia) followed by thrombin (Sigma) digestion. Thrombin was removed after column chromatography on Q column (GE) by elution with QA buffer [50 mM Tris-HCl pH 7.5, 1 mM EDTA, 1 mM PMSF, and 1 mM dithiothreitol (DTT)]. *Candida albican*s *Cdc8* was cloned into pGEX-2T plasmid and transformed into *E. coli BL21* strain. Purification of Cdc8 protein was carried out by a procedure similar to that described above.

Isothermal titration calorimetry. The ITC measurements were conducted on a MicroCal Microcalorimeter from GE Healthcare Bio-Sciences AB (Uppsala, Sweden). Compound **1c** (50 μL of 1.228 mM PBS solution containing 50% glycerol, pH 7.4) was added into hTMPK (0.0817 mM of PBS solution containing 50% glycerol) by the designated portions (initial injection volume is 0.5 μL, the other injection volume is 2 μL, and the space time is 4 min) at 298 K with continuous stirring (1000 rpm). Origin™ software is then used to analyze the ITC data using fitting models to calculate reaction stoichiometry (n), binding constant (K_{ass}), enthalpy (ΔH) and entropy (ΔS).

Luciferase-coupled TMPK assay. The test compound was stored as 10 mM in DMSO solution at –20 ^{o}C, and diluted with H_2O to 10 μM for bioassay. The TMPK reaction was started by addition of purified hTMPK (10 μL of 0.1 μg/μL in PBS buffer, pH 7.4) and the test compound (10 μL of 10 μM solution) to the TMPK assay buffer (15 μL of 100 mM Tris-HCl solution, pH 7.5, containing 100 mM KCl, 10 mM $MgCl_2$, 5 μM ATP and 100 μM

dTMP) in 96-well plate at 25 ^{o}C for 10 min. The mixture was then transferred to a white 96-well plate containing 15 μL of CellTiter-Glo (50% in DMEM buffer). The luminescence was measured with a luminescence counter (Packard).

NADH-coupled TMPK assay. All reactions were performed in 96-well plates in an assay volume of 100 μL. The activity of hTMPK was measured at 25 ^{o}C using a modified NADH-coupled colorimetric assay as described previously,[37] in which purified hTMPK was added to buffer containing 100 mM Tris-HCl (pH 7.5), 100 mM KCl, 10 mM $MgCl_2$, 500 μM ATP, 250 μM TMP/CMP, 500 μM phosphoenol pyruvate, 250 μM NADH, pyruvate kinase (4 units) and lactate dehydrogenase (5 units). After 20 min, the change of NADH was detected by reading at OD 340 nm.

Tyrosine kinase assay. The activity of tyrosine kinase (TK) is measured by using Universal Tyrosine Kinase Assay Kit (Takara Bio Inc.). The kinase reacting solution, TK substrate immobilized microplate, extraction buffer, and blocking solution are provided by this kit. The test compound was stored as 10 mM in DMSO solution, and diluted with H_2O to 5 mM for assay. Total proteins were extracted from MB-231 cells after incubation for 1 day. Tyrosine kinase was collected by immunoprecipitation. The immune-precipitates were washed by PBS (pH = 7.4) for three times. The precipitates were suspended in 150 μL of kinase reacting solution containing 10 mM 2-mercaptoethanol to give TK solution (3000 × 10^{-5} units/μL). The TK solution was diluted to 30×, and 85.8 μL of the diluted TK solution

was mixed with test compound (2.2 μL of 5 mM solution). An aliquot of the mixture (40 μL) and ATP-2Na (10 μL of 40 mM solution in H_2O) was added to TK substrate immobilized microplate. After incubation of the mixture at 37 ℃ for 30 min, the sample solution was removed and washed 4 times by washing buffer (PBS buffer contain 0.05% (v/v) Tween20). Bolcking solution (100 μL) was added into each well and incubated for 30 min at 37 ℃. Bolcking solution was removed and anti-phosphotyrosine (PY20)–HRP solution (50 μL) was added. After incubation for 30 min at 37 ℃, the antibody solution was removed and each well was washed for 4 times with washing buffer. HRP substrate solution (100 μL) was added. After 15 min incubation, 1 M H_2SO_4 aqueous solution was added to stop the reaction. The absorbance at 450 nm was recorded by plate reader to determinate the TK activity.

^{32}P-Phosphate transfer assay. After preincubation with **1a** at the indicated concentration for 10 min, human TMPK (0.2 μg) or candida Cdc8 (0.02 μg) was added to a TMPK reaction mixture containing 0.05 μM [γ-^{32}P] ATP (10 μCi/uL), 50 μM ATP, 50 μM dTMP, 100 mM Tris-HCl, 100 mM KCl and 10 mM $MgCl_2$. The assay was terminated by heating and addition of 20 mM dTMP, dTDP and dTTP. Two microliter of the reaction mixture was spotted onto polyethyleneimine (PEI)-cellulose thin-layer chromatography (TLC) for separation by 2 M acetic acid/ 0.5M LiCl. The position of dTMP, dTDP and dTTP on TLC sheet was visualized by UV, followed by autoradiography. The spots corresponding to ^{32}P-dTDP were excised for radioactivity measurement by β-scintillation counter (Beckman).

Cell viability assay. IL-3-dependent 32D cells and the Bcr-Abl/32D cells were grown in RPMI 1640 medium supplemented with 10% FBS, 2 mM glutamine, penicillin/streptomycin, and 25% WEHI media. Wehi3b cells were maintained in RPMI 1640 medium supplemented with 10% FBS, 2 mM glutamine, penicillin/streptomycin. All cells were incubated with 5% CO_2 at 37 ^{o}C. 32D, Bcr-Abl/32D and Wehi3b cells were kindly provided by Ralph B. Arlinghaus (the Department of Translational Molecular Pathology, University of Texas M.D. Anderson Cancer Center, Houston, Texas, USA). Cells were plated into a 96-well plate (10^3 cells/well). After 3 days, cell viability was measured by the WST-1 assays (Roche, Germany).[38]

Western blot analysis. An incubation solution containing probe **4** (6.8 μL of 3 mM solution in DMSO), purified hTMPK (21 μL of 1.16 μg/μL in 1× PBS) and 50× protease inhibitor cocktail (cOmplete™, 20 μL aqueous solution, Roche) was made up to 1 mL total volume in 1× PBS buffer (pH 7.4). After incubation at 25 ^{o}C for 30 min, the mixture was irradiated with 254-nm UV light for three times (1 min duration each time). An aliquot (20 μL) of the photolabeled product mixture was taken and added to 2× sample buffer (20 μL containing 4% sodium dodecyl sulfate (SDS), 20% glycerol, 10% 2-mercaptoethanol, 0.004% bromphenol blue and 0.125 M Tris-HCl, pH ≈ 6.8). After boiling at 95 ^{o}C for 10 min, the mixture was allowed to cool to room temperature before loading on a denature 12% SDS polyacrylamide gel electrophoresis (SDS–PAGE). After electrophoresis, the photolabeled

protein was transferred to polyvinylidene difluoride (PVDF) membrane and treated with streptavidin-conjugated horseradish peroxidase, followed by visualization with chemiluminescence (BioSpectrum 600 imaging system, UVP).

Proteolytic digestion of labeled hTMPK. To map the modification regions of hTMPK by photoaffinity probe **4**, labeled hTMPK was subjected to proteolytic digestion by trypsin and chymotrypsin, separately. To remove excess free probe, labeled hTMPK solution (60–70 μg protein) was dialyzed twice against water using Slide-A-Lyzer MINI (3500 Da MWCO, Thermo Pierce). For denaturation, protein solution was dialyzed twice against 25 mM ammonium bicarbonate buffer containing 6.5 M urea (pH ≈ 8) for trypsin, or 100 mM Tris-HCl buffer containing 10 mM $CaCl_2$ and 6.5 M urea (pH ≈ 8) for chymotrypsin. After dialysis, the sample was reduced and alkylated by adding 5 mM DTT, heating at 95 ^{o}C for 10 min, adding 35 mM iodoacetamide, incubating at room temperature in the dark for 30 min, adding 25 mM DTT, and incubating at room temperature for 10 min. The resulting hTMPK solution was diluted by adding corresponding buffers without urea to reduce urea to <1 M prior to digestion. hTMPK was digested by trypsin (1:50, w/w) or chymotrypsin (1:100, w/w) at 37 ^{o}C for 16 h. An aliquot of digested peptides was desalted by C18 ZipTip (Millipore) for LC–MS/MS analysis. The remaining aliquot was subjected to avidin affinity chromatography.

Monomeric avidin affinity enrichment of biotinylated peptides. Monomeric avidin agarose (Thermo Pierce) was used to enrich biotinylated peptides of labeled hTMPK

according to manufacturer's protocols. Briefly, the settled resin was washed with PBS three times and incubated with 2 mM D-biotin in PBS to block non-reversible biotin binding sites. This was followed by incubation in 0.1 M glycine (pH 2.5) solution for 10 min to recover reversible biotin binding sites, and washed with PBS three times. hTMPK peptides were incubated with the resin for 2 h at room temperature. After washing with PBS four times, 0.1 M glycine (pH 2.5) solution was added to elute biotinylated peptides for 30 min at room temperature. The elution fraction was lyophilized and desalted by C18 ZipTip for LC–MS/MS analysis.

Proteolytic digestion of labeled hTMPK without denaturation and reduction. The test compound (**1a**, **A** or DTNB, 20 μL of 10 mM solution in DMSO) and purified hTMPK (10 μL of 2.47 μg/μL in PBS) was made up to 1 mL total volume in PBS buffer (pH 7.4). Each sample was incubated at 25 ^{o}C for 30 min, and an aliquot (200 μL) was dialyzed twice against water using Slide-A-Lyzer MINI (3500 Da MWCO) to remove excess compound. Labeled hTMPK was digested by trypsin (1:50, w/w) at 37 ^{o}C for 12 h. An aliquot of digested peptides was desalted by C18 ZipTip (Millipore) for LC–MS/MS analysis.

ESI/LC–MS/MS analysis. LC–MS/MS was conducted on Waters ACQUITY nanoUPLC system conjugated with Waters Synapt G2 HDMS (Milford, MA, USA). Waters C18 column (1.7 μm BEH130 C18, 75 μm × 250 mm) was eluted with a gradient of 6–60% acetonitrile (with 0.1% formic acid) over 70 min at 0.3 μL/min. ESI cone voltage was 2.8 kV.

Spectra were acquired every 0.024 sec, covering the mass range 350–1750 Da and accumulating for 0.5 sec per cycle. Collision-induced dissociation spectra were acquired by setting the MS1 quadrupole to transmit a precursor mass window of ±100 mDa centered on the five most abundant isotopomers in the charge states of +2, +3, and +4. Argon was the collision gas, and the collision energy was dependent on charge state and molecular weight of precursor ions. Spectra were acquired every 0.024 sec covering the mass range 100–1990 Da while accumulating data for 0.7 sec per cycle.

Synthetic procedures and compound characterization. Benzo[*d*]isothiazol-3[2*H*]-one (**6c**) is commercially available. Compound **1a** was synthesized according to our previously reported procedure.[2] The purity of compounds **1a**–**4**, was determined to be >95% by HPLC on a reversed-phase HC-C18 column (Agilent, 4.6 × 250 mm, 5 μm) or a Platisil column (Dikma, 4.6 × 250 mm, 5 μm).

2-Mercapto-4,6-dimethylnicotinonitrile (5a). A mixture of 2-chloro-4,6-dimethylnicotinonitrile (0.6 g, 3.6 mmol) and thiourea (0.9 g, 11.7 mmol) in *n*-butanol (24 mL) was heated at reflux (118 ^{o}C) for 4 h. After cooling to room temperature, the solution turned to a suspension containing light yellow solids. The solids were collected by filtration, rinsed with *n*-butanol, and dried under reduced pressure to give 2-mercapto-4,6-dimethylnicotinonitrile (**5a**, 125 mg, 99% yield). $C_8H_8N_2S$; light yellow powder; mp 223–225 ^{o}C; ^{1}H NMR (400 MHz, DMSO-d_6) δ 6.69 (1 H, s), 3.32 (1 H, s), 2.34

(6 H, s); ^{13}C NMR (100 MHz, DMSO-d_6) δ 177.5, 156.8, 152.6, 116.2, 114.8, 113.4, 20.8, 18.8; ESI–HRMS calcd for $C_8H_9N_2S$: 165.0486, found: *m/z* 165.0491$[M + H]^+$.

2-Mercaptonicotinonitrile (5b). A mixture of 2-chloronicotinonitrile (200 mg, 1.44 mmol) and thiourea (310 mg, 4.33 mmol) in *n*-butanol (5 mL) was heated at reflux (118 ^{o}C) for 4 h. After cooling to room temperature, the solution turned to a suspension containing light yellow solids. The solids were collected by filtration, rinsed with *n*-butanol, and dried under reduced pressure to give 2-mercaptonicotinonitrile (**5b**, 144 mg, 73% yield). $C_6H_3N_2S$; yellow powder; mp 202–203 ^{o}C; ^{1}H NMR (400 MHz, CD_3OD) δ 7.96 (1 H, dd, *J* = 7.6, 2.0 Hz), 7.81 (1 H, dd, *J* = 6.4, 2.0 Hz), 6.83 (1 H, td, *J* = 7.2, 1.2 Hz); ^{13}C NMR (100 MHz, DMSO-d_6) δ 177.3, 145.5, 142.7, 116.8, 116.6, 112.3; ESI–HRMS calcd for $C_6H_3N_2S$: 135.0017, found: *m/z* 135.0016 $[M – H]^–$.

4-Bromo-2-mercaptobenzonitrile (5d). A mixture of 4-bromo-2-fluorobenzonitrile (2.00 g, 10 mmol) and Na_2S (0.93, 12 mmol) in DMF (10 mL) was stirred at room temperature for 15 h. After addition of 1 M NaOH (70 mL), the mixture was washed with CH_2Cl_2 (4 × 30 mL). The aqueous layer was acidified with 6 M HCl to pH 1–2 and extracted with CH_2Cl_2. The combined organic layer was washed with brine, dried over $MgSO_4$, filtered, and concentrated under reduced pressure to give 4-bromo-2-mercaptobenzonitrile (**5d**, 2.01 g, 93% yield). C_7H_4BrNS; yellow solid; mp 106–107 ^{o}C; ^{1}H NMR (400 MHz, $CDCl_3$) δ 7.57 (1 H, d, *J* = 1.6 Hz), 7.44 (1 H, d, *J* = 8.4 Hz), 7.36 (1 H, dd, *J* = 8.0, 1.6 Hz), 4.11 (1 H, s); ^{13}C NMR (100

MHz, $CDCl_3$) δ 139.4, 134.2, 131.9, 129.1, 127.9, 116.8, 110.5; ESI−HRMS calcd for C_7H_3BrNS: 211.9170, found: *m/z* 211.9179 $[M - H]^-$.

4,6-Dimethylisothiazolo[5,4-*b*]pyridin-3(2*H*)-one (6a). A solution of thiol compound **5a** (601 mg, 3.66 mmol) in conc. H_2SO_4 (5 mL) was stirred at 100 ^oC for 4 h. The mixture was cooled and adjusted to pH 5–6 by addition of saturated $NaHCO_{3(aq)}$ to produce white solids in suspension. The solids were collected by filtration, rinsed with H_2O, and dried under reduced pressure to give compound **6a**, (400 mg, 61% yield). $C_8H_8N_2OS$; off-white solid; mp 191–193 ^oC; ^1H NMR (400 MHz, $CDCl_3$) δ 6.96 (1 H, s), 2.75 (3 H, s), 2.62 (3 H, s); ^{13}C NMR (100 MHz, $CDCl_3$) δ 168.1, 166.4, 163.3, 149.8, 122.4, 114.7, 24.6, 17.8; ESI–HRMS calcd for $C_8H_9N_2OS$: 181.0436, found: *m/z* 181.0441 $[M + H]^+$.

Isothiazolo[5,4-*b*]pyridin-3(2*H*)-one (6b). A solution of thiol compound **5b** (1000 mg, 7.34 mmol) in conc. H_2SO_4 (8 mL) was stirred at 100 ^oC for 4 h. The mixture was cooled and adjusted to pH 5–6 by addition of saturated $NaHCO_{3(aq)}$ to produce yellow solids in suspension. The solids were collected by filtration, rinsed with H_2O, and dried under reduced pressure to give compound **6b** (333 mg, 30% yield). $C_6H_3N_2OS$; yellow powder; mp 170–171 ^oC; IR ν_{max} (neat) 3415, 2916, 2872, 2345, 2304, 1659, 1585, 1560, 1377, 1102, 952, 770,500 cm^{-1}; ^1H NMR (400 MHz, $CDCl_3$) δ 8.81 (1 H, dd, *J* = 4.8, 1.6 Hz), 8.33 (1 H, dd, *J* = 7.6, 1.6 Hz), 7.40 (1 H, dd, *J* = 7.6, 4.4 Hz); ^{13}C NMR (100 MHz, *d*-DMSO) δ163.7, 153.2, 133.8,

120.9 (2 ×), 118.9; ESI–HRMS calcd for $C_6H_3N_2OS$: 150.9966, found: *m/z* 150.9965 [M – H]$^-$.

6-Bromobenzo[*d*]isothiazol-3(2*H*)-one (6d). The above-prepared compound **5d** (600 mg, 2.80 mmol) was added to conc. H_2SO_4 (5 mL). The mixture was immersed in a preheated oil bath at 100 ^oC for 5 h, and then cooled. The mixture was modulated to pH 5–6 by addition of saturated $NaHCO_3$ to produce insoluble substance in suspension. The solids were collected by filtration, and dried under reduced pressure to give 6-bromobenzo[*d*]isothiazol-3(2*H*)-one (**6d**, 603 mg, 94% yield). C_7H_4BrNOS; yellow powder; mp 194–196 ^oC; IR ν_{max} (neat) 2922, 2851, 1716, 1575, 1541, 1368, 1286, 1267, 1245, 1087, 1048, 978, 816, 663 cm^{-1}; ^{1}H NMR (400 MHz, CD_3OD) δ 7.98 (1 H, s), 7.75 (1 H, d, *J* = 8 Hz), 7.49 (1 H, dd, *J* = 8.4, 1.6 Hz); ^{13}C NMR (100 MHz, DMSO-d_6) δ 164.0, 150.0, 128.0, 125.5, 124.1, 123.9 (2 ×); ESI−HRMS (negative mode) calcd for C_7H_3BrNOS: 227.9119, found: *m/z* 227.9130 [M − H]$^-$.

***Tert*-butyl 4-(2-iodoacetyl)piperazine-1-carboxylate (7).** A mixture of piperazine (1.10 g, 12.8 mmol) and DIEA (2.24 mL, 12.8 mmol) in anhydrous CH_2Cl_2 (60 mL) was stirred at room temperature, and a solution of di-*tert*-butyl dicarbonate (1.46 mL, 6.4 mmol) in anhydrous CH_2Cl_2 (80 mL) was added slowly via a separatory funnel over a period of 3 h. The mixture was extracted with CH_2Cl_2 and H_2O. The organic phase was dried over $MgSO_4$, filtered, and concentrated to give mono-Boc protected piperazine (2.01 g, 85% yield).

A mixture of the above-prepared compound (1.24 g, 6.64 mmol), chloroacetyl chloride

(0.63 mL, 7.32 mmol) and DIEA (3.5 mL, 19.94 mmol) in anhydrous CH_2Cl_2 was stirred at room temperature for 4 h. The mixture was extracted with CH_2Cl_2 and H_2O. The organic phase was dried over $MgSO_4$, filtered, and purified by flash chromatography on a silica gel column with elution of EtOAc/hexane (1:2) to give *tert*-butyl 4-(2-chloroacetyl)piperazine-1-carboxylate (1.14 g, 71% yield). $C_{11}H_{19}ClN_2O_3$; white solid; mp 68–70 ^oC; ^1H NMR (400 MHz, $CDCl_3$) δ 4.05 (2 H, s), 3.56–3.58 (2 H, m), 3.47 (4 H, s), 3.42–3.43 (2 H, m), 1.45 (9 H, s); ^{13}C NMR (100 MHz, $CDCl_3$) δ 164.8, 154.0, 80.1, 45.9, 43.1 (2 ×), 41.8, 40.7, 28.2 (3×); ESI–HRMS calcd for $C_{11}H_{20}ClN_2O_3$: 263.1162, found: *m/z* 263.1165 $[M + H]^+$.

A mixture of the above-prepared chloro compound (913 mg, 3.48 mmol) and sodium iodide (1.58 g, 10.53 mmol) in acetone (35 mL) was stirred at room temperature for 16 h. The solids were removed by filtration, and the solution was concentrated under reduced pressure. The residue was extracted with CH_2Cl_2 and H_2O. The organic phase was dried over $MgSO_4$, filtered, and concentrated to give *tert*-butyl 4-(2-iodoacetyl)piperazine-1-carboxylate (**7**, 1.13 g, 92% yield). $C_{11}H_{19}IN_2O_3$; brown solid; mp 69–71 ^oC; IR ν_{max} (neat) 2976, 2929, 2861, 1696, 1650, 1459, 1419, 1366, 1258, 1168, 996, 750 cm^{-1}; ^1H NMR (400 MHz, $CDCl_3$) δ 3.74 (2 H, s), 3.56–3.59 (2 H, m), 3.51–3.53 (2 H, m), 3.40–3.42 (4 H, m), 1.46 (9 H, s); ^{13}C NMR (100 MHz, $CDCl_3$) δ 166.2, 153.9, 80.1, 46.8, 42.6 (2 ×), 41.7, 28.2 (3 ×), –4.0; ESI–HRMS calcd for $C_{11}H_{20}IN_2O_3$: 355.0519, found: *m/z* 355.0515 $[M + H]^+$.

***Tert*-butyl 4-(2-(4,6-dimethyl-3-oxoisothiazolo[5,4-*b*]pyridin-2(3*H*)-yl)acetyl) piperazine-1-carboxylate (1b).** Isothiazolone **6a** (300 mg, 1.66 mmol) was added to a suspension of iodo compound **7** (578 mg, 1.66 mmol), Et_3N (1.16 mL, 8.30 mmol) and Cs_2CO_3 (500 mg, 1.54 mmol) in anhydrous CH_2Cl_2 (25 mL) at room temperature. The mixture was stirred for 24 h, and concentrated under reduced pressure. The residue was extracted with CH_2Cl_2 and H_2O. The organic phase was dried over $MgSO_4$, filtered, concentrated, and purified by flash chromatography on a silica gel column with elution of EtOAc/hexane (1:1) to give compound **1b** (400 mg, 59% yield). The purity of product **1b** was 98.4% as shown by HPLC on an HC-C18 column (Agilent, 4.6 × 250 mm, 5 μm), t_R = 8.1 min (gradients of 40−90% aqueous CH_3CN in 15 min). $C_{19}H_{26}N_4O_4S$; white solid; mp 204−207 ^oC; IR ν_{max} (neat) 3473, 2974, 2924, 1655, 1588, 1564, 1460, 1419, 1365, 1286, 1238, 1169, 1127, 1033, 997, 765 cm^{-1}; ^1H NMR (400 MHz, $CDCl_3$) δ 6.89 (1 H, s), 4.62 (2 H, s), 3.56 (2 H, m), 3.47 (2 H, m), 3.41 (4 H, m), 2.67 (3 H, s), 2.55 (3 H, s), 1.42 (9 H, s); ^{13}C NMR (100 MHz, $CDCl_3$) δ 164.8, 164.7, 163.1, 162.9, 154.1, 149.7, 122.4, 113.9, 80.35, 45.0, 44.3, 43.1 (2 ×), 42.0, 28.4 (3 ×), 24.6, 17.5; ESI−HRMS calcd for $C_{19}H_{26}N_4O_4S$: 407.1753, found: *m/z* 407.1756 $[M + H]^+$.

***Tert*-butyl-4-(2-(3-oxoisothiazolo[5,4-*b*]pyridin-2(3*H*)-yl)acetyl)piperazine-1-carboxylate (2b).** A mixture of the-above prepared isothiazolo[5,4-*b*]pyridin-3(2*H*)-one **6b** (500 mg, 3.29 mmol), iodo compound **7** (1.17 mg, 3.29 mmol), Cs_2CO_3 (1.07 mg, 3.29 mmol)

and Et_3N (2.28 mL, 16.45 mmol) in CH_2Cl_2 (20 mL) was stirred for 5 h at room temperature. The mixture was concentrated under reduced pressure, and then purified by flash chromatography on a silica gel column with elution of EtOAc/hexane (1:1 to EA) to give compound **2b** (910 mg, 40% yield). The purity of product **2b** was 98.3% as shown by HPLC on DIKMA column (Agilent, 4.6 × 250 mm, 5 μm), t_R = 9.5 min (elution of EtOAc in 20 min). $C_{17}H_{23}N_4O_4S$; yellow solid; mp 168-169°C; IR ν_{max} (neat) 3515, 2976, 2929, 2865, 2390, 2353, 1665, 1586, 1564, 1462, 1415, 1395, 1365, 1286, 1235, 1168, 1127, 1028, 996, 863, 761, 557 cm^{-1}; ^1H NMR (400 MHz, $CDCl_3$) δ 8.77 (1 H, dd, *J* = 4.4, 1.6 Hz), 8.28 (1 H, dd, *J* = 8.0, 2.0 Hz), 7.35 (1 H, dd, *J* = 7.6, 4.4 Hz), 4.71 (2 H, s), 3.62–3.59 (2 H, m), 3.52–3.42 (6 H, m) 1.45 (9 H, s); ^{13}C NMR (100 MHz, $CDCl_3$) δ 164.8, 164.2, 163.3, 154.4, 154.0, 134.9, 120.6, 118.3, 80.6, 45.0 (2 ×), 44.5, 42.0 (2 ×), 28.3 (3 ×); ESI–HRMS calcd for $C_{17}H_{23}N_4O_4S$: 379.1440, found: *m/z* 379.1438 $[M + H]^+$.

***Tert*-butyl 4-(2-(3-oxobenzo[*d*]isothiazol-2(3*H*)-yl)acetyl)piperazine-1-carboxylate (3b).** A mixture of benzo[*d*]isothiazol-3(2*H*)-one (**6c**, 1.20 g, 7.94 mmol), iodo compound **7** (2.80 g, 7.95 mmol), Et_3N (5.4 mL, 38.7 mmol) and Cs_2CO_3 (3.88 g, 11.9 mmol) in CH_2Cl_2 (123 mL) was stirred for 5 h at room temperature. The mixture was stirred for 4 h, and then extracted with CH_2Cl_2 and H_2O. The combined organic phase was washed with brine, dried over $MgSO_4$ and concentrated under reduced pressure. After flash column chromatography (silica gel, hexane/EtOAc (1:1 to 1:2)), the product **3b** was obtained (1.60 g, 60% yield). The

purity of product **3b** was 96.9% as shown by HPLC on an HC-C18 column (Agilent, 4.6 × 250mm, 5 μM), t_R = 16.6 min (gradients of 20−90% aqueous CH_3CN in 20 min). $C_{18}H_{23}N_3O_2S$; white solid, mp 169–170 ^oC; IR ν_{max} (neat) 2974, 2925, 1655, 1460, 1418, 1364, 1339, 1285, 1171, 1128, 1068, 1028 740 cm^{-1}; ^1H NMR (400 MHz, $CDCl_3$) δ 8.01 (1 H, d, *J* = 7.7 Hz), 7.60 (1 H, td, *J* = 7.7, 0.8 Hz), 7.53 (1 H, d, *J* = 7.7 Hz), 7.38 (1 H, t, *J* = 7.7 Hz), 4.68 (2 H, s), 3.58 (2 H, m), 3.52 (2 H, m), 3.42–3.40 (4 H, m), 1.43 (9 H, s); ^{13}C NMR (100 MHz, $CDCl_3$) δ 165.6, 165.1, 154.3, 141.2, 132.1, 126.7, 125.4, 123.2, 120.3, 80.3, 45.0, 44.7 (2 ×), 41.9 (2 ×), 28.2 (3 ×); ESI–HRMS calcd for $C_{18}H_{24}N_3O_4S$: 378.1488, found *m/z* 378.1488 $[M + H]^+$.

4,6-Dimethyl-2-(2-oxo-2-(piperazin-1-yl)ethyl)isothiazolo[5,4-*b*]pyridin-3(2*H*)-one (1c). Compound **1b** (20 mg, 0.05 mmol) and TFA (4 mL, 52.6 mmol) was dissolved in anhydrous CH_2Cl_2 (15 mL), and then stirred for 0.5 h at 27 ^oC. TFA was removed under reduced pressure, and the residue was extracted with ammonia solution (35%) and CH_2Cl_2. The organic layer was dried over $MgSO_4$, filtered, and concentrated to give compound **1c** (16 mg, 100% yield). The purity of product **1c** was 95.2% as shown by HPLC on an HC-C18 column (Agilent, 4.6 × 250 mm, 5 μm), t_R = 3.9 min (gradients of 20−90% aqueous CH_3CN in 15 min). $C_{14}H_{18}N_4O_2S$; white solid; mp 175−177 ^oC; IR ν_{max} (neat) 3475, 3310, 2925, 1652, 1565, 1443, 1337, 1275, 1033, 750 cm^{-1}; ^1H NMR (400 MHz, $CDCl_3$) δ 6.92 (1 H, S), 4.64 (2 H, s), 3.62 (2 H, m), 3.53 (2 H, m), 2.88 (4 H, m), 2.72 (3 H, s), 2.59 (3 H, s), 2.04 (1 H, s);

^{13}C NMR (100 MHz, $CDCl_3$) δ 164.4, 164.1, 162.9, 162.4, 149.4, 122.6, 113.9, 46.5, 46.3, 45.9, 44.4, 43.5, 24.9, 17.9; ESI−HRMS calcd for $C_{14}H_{19}N_4O_2S$: 307.1229, found: *m/z* 307.1227 $[M + H]^+$.

***Tert*-butyl 4-(2-(6-bromo-3-oxobenzo[*d*]isothiazol-2(3*H*)-yl)acetyl)piperazine-1-carboxylate (8).** A mixture of the above-prepared compound **6d** (760 mg, 3.32 mmol), iodine compound **7** (1293 mg, 3.65 mmol) and DIEA (1.72 mL, 9.96 mmol) in THF (20 mL) was stirred for 4 h at room temperature. The mixture was concentrated under reduced pressure. The residue was extracted with CH_2Cl_2 and H_2O. The organic phase was dried over $MgSO_4$, filtered, concentrated, and purified by flash chromatography on a silica gel column with elution of EtOAc/hexane (1:1) to give compound **8** (622 mg, 41% yield). $C_{18}H_{22}BrN_3O_4S$; yellow solid; mp 193–195 ^oC; IR ν_{max} (neat) 2975, 2925, 2860, 1654, 1588, 1457, 1418, 1365, 1286, 1235, 1168, 1127, 1028, 996, 666 cm^{-1}; ^{1}H NMR (400 MHz, $CDCl_3$) δ 7.86 (1 H, d, *J* = 8.4 Hz), 7.71 (1 H, d, *J* = 1.2 Hz), 7.50 (1 H, dd, *J* = 8.4, 1.2 Hz), 4.66 (2 H, s), 3.58–3.57 (2 H, m), 3.51–3.50 (2 H, m), 3.46–3.41 (4 H, m), 1.45 (9 H, s); ^{13}C NMR (100 MHz, $CDCl_3$) δ 165.0 (2 ×), 154.4, 143.0, 129.1, 127.9, 127.1, 123.0, 122.2, 80.5, 45.1 (2 ×), 44.8, 42.0 (2 ×), 28.3 (3 ×); ESI−HRMS calcd for $C_{18}H_{23}BrN_3O_4S$: 456.0593, found: *m/z* 456.0591 $[M + H]^+$.

***Tert*-butyl 4-(2-(6-amino-3-oxobenzo[*d*]isothiazol-2(3*H*)-yl)acetyl)piperazine-1-**

carboxylate (9) and *tert*-butyl 4-(2-(6-azido-3-oxobenzo[*d*]isothiazol-2(3*H*)-yl)acetyl) piperazine-1-carboxylate (10). Under an atmosphere of argon, a mixture of bromine compound **8** (200 mg, 0.44 mmol), NaN_3 (57 mg, 0.88 mmol), CuI (33 mg, 0.18 mmol) and sodium ascorbate (17 mg, 0.09 mmol) in EtOH/H_2O (7:3, 4mL) was stirred at room temperature. After addition of DMEDA (0.03 mL, 0.26 mmol), the temperature was elevated to 100 ^oC for 2 h, and then concentrated under reduced pressure. The residue was extracted with EtOAc and H_2O. The organic phase was dried over $MgSO_4$, filtered, concentrated, and separated by chromatography on a silica gel column with elution of EtOAc/hexane (1:1) to give the azido compound **10** (23 mg, 12% yield) along with the aniline compound **9** (100 mg, 58% yield).

Aniline compound **9** (79 mg, 0.20 mmol) and *N*-methyl-2-pyrrolidonium bisulfate (198 mg, 1.0 mmol) was dissolved in H_2O (2 mL), and stirred for 10 min. To this solution was added sodium nitrite (44 mg, 0.63 mmol) over a period of 3 min. Upon completion of the addition, the mixture was stirred for an additional 15 min. Sodium azide (41 mg, 0.63 mmol) was added over a period of 5 min. After 1 h, the solids were collected by filtration, rinsed with 10% HCl, and dried under reduced pressure to give the azido compound **10** (38 mg; 45%).

Compound **9**: $C_{18}H_{24}N_4O_4S$; yellow solid; mp 178–180 ^oC; ^1H NMR (400 MHz, $CDCl_3$) δ 7.73 (1 H, d, J = 8.4 Hz), 6.64 (2 H, m), 4.60 (2 H, s), 3.57–3.56 (2 H, m), 3.52–3.49 (2 H,

m), 3.44–3.39 (4 H, m), 1.45 (9 H, s); ^{13}C NMR (100 MHz, $CDCl_3$) δ 165.8, 165.7, 154.4, 150.7, 143.7, 127.9, 114.1 (2 ×), 103.1, 80.4, 45.2 (2 ×), 44.8, 42.0 (2 ×), 28.3 (3 ×); ESI−HRMS calcd for $C_{18}H_{24}N_4O_4S$: 393.1597, found: *m/z* 393.1597 $[M + H]^+$.

Compound **10**: $C_{18}H_{22}N_6O_4S$; yellow solid; mp 174–176 °C; IR ν_{max} (neat) 2977, 2929, 2866, 2110, 1697, 1655, 1601, 1467, 1420, 1366, 1287, 1237, 1169, 1126, 1029, 996, 735, 671 cm^{-1}; ^{1}H NMR (400 MHz, $CDCl_3$) δ 7.99 (1 H, d, *J* = 8.4 Hz), 7.15 (1 H, d, *J* = 2.0 Hz), 7.05 (1 H, dd, *J* = 8.4, 2.0 Hz), 4.66 (2 H, s), 3.60–3.58 (2 H, m), 3.53–3.51 (2 H, m), 3.45–3.42 (4 H, m), 1.46 (9 H, s); ^{13}C NMR (100 MHz, $CDCl_3$) δ 165.2, 165.0, 154.4, 144.8, 143.3, 128.3, 120.2, 117.2, 110.0, 80.5, 45.1 (2 ×), 44.8, 42.0 (2 ×), 28.3 (3 ×); ESI−HRMS calcd for $C_{18}H_{23}N_6O_4S$: 419.1503, found: *m/z* 419.1502 $[M + H]^+$.

6-Azido-2-(2-oxo-2-(piperazin-1-yl)ethyl)benzo[*d*]isothiazol-3(2*H*)-one (11). Compound **10** (140 mg, 0.34 mmol) and TFA (5.1 mL, 67 mmol) was dissolved in CH_2Cl_2 (20 mL), and then stirred for 0.5 h at 25 °C. TFA was removed under reduced pressure, and compound **11** (127 mg; 87%) was obtained. $C_{13}H_{14}N_6O_2S$; light yellow oil; IR ν_{max} (neat) 2910, 2851, 2130, 1683, 1653, 1472, 1201, 1130, 721, 672 cm^{-1}; ^{1}H NMR (400 MHz, CD_3OD) δ 7.95 (1 H, d, *J* = 8.4 Hz), 7.53 (1 H, d, *J* = 2.0 Hz), 7.15 (1 H, dd, *J* = 8.4, 2.0 Hz), 4.84 (2 H, s), 3.86–3.84 (4 H, m), 3.35 (2 H, m), 3.26 (2 H, m); ^{13}C NMR (100 MHz, CD_3OD) δ 167.4 (2 ×), 146.6, 145.3, 128.7, 121.7, 118.8, 112.0, 45.9 (2 ×), 44.4, 43.1, 40.2; ESI−HRMS calcd for $C_{13}H_{15}N_6O_2S$: 319.0977, found: *m/z* 319.0977 $[M + H]^+$.

2-(2-(2-Iodoethoxy)ethoxy)ethyl 5-((3a*S*,4*S*,6a*R*)-2-oxohexahydro-1*H*-thieno[3,4-*d*]imidazol-4-yl)pentanoate (12). Under an atmosphere of N_2, NaH (44 mg, 1.1 mmol) was added to a solution of biotin (244 mg, 1 mmol) in DMSO (5 ml). The mixture was stirred for 10 min at room temperature, and added 1,2-bis(2-iodoethoxy)ethane (555 mg, 1.5 mmol) dropwise. The mixture was stirred for 14 h, and then quenched by adding half-saturated $NH_4Cl_{(aq)}$. The mixture was extracted with EtOAc, and dried under reduced pressure. The residue was purified by silica gel column chromatography with elution of hexane/EtOAc (3:1) to give compound **12** (286 mg, 60%). $C_{16}H_{27}N_2O_5SI$; white solid; mp 122–125 ^oC; $[\alpha]^{25}_D$ = +45.6 (*c* = 1.0, $CHCl_3$); lit: $[\alpha]^{25}_D$ = +31.0 (*c* = 1.0, $CHCl_3$); IR ν_{max} (neat) 3223, 2920, 1703, 1463, 1263, 1117, 1034, 861, 762 cm^{-1}; ^1H NMR (400 MHz, $CDCl_3$) δ 5.75 (1 H, s), 5.19 (1 H, s), 4.50–4.47 (1 H, m), 4.31–4.27 (1 H, m), 4.23–4.20 (2 H, m), 3.75 (2 H, t, *J* = 7.2 Hz), 3.70 (2 H, t, *J* = 4.4 Hz), 3.64 (4 H, s), 3.26 (2 H, t, *J* = 7.2 Hz), 3.16–3.11 (1 H, m), 2.91–2.87 (1 H, dd, *J* = 12.8, 5.2 Hz), 2.73 (1 H, d, *J* = 12.8 Hz), 2.37 (2 H, t, *J* = 7.6 Hz), 1.71–1.62 (4 H, m), 1.46–1.40 (2 H, m); ^{13}C NMR (100 MHz, $CDCl_3$) δ 173.6, 163.4, 71.9, 70.5, 70.2, 69.2, 63.4, 61.9, 60.1, 55.4, 40.5, 33.8, 28.3, 28.2, 24.7, 2.9; ESI−HRMS calcd for $C_{16}H_{28}N_2O_5SI$: 487.0762, found: *m/z* 487.0762 $[M + H]^+$.

2-(2-(2-(4-(2-(6-Azido-3-oxobenzo[*d*]isothiazol-2(3*H*)-yl)acetyl)piperazin-1-yl) ethoxy)ethoxy)ethyl 5-((3a*S*,4*S*,6a*R*)-2-oxohexahydro-1*H*-

thieno[3,4-*d*]imidazol-4-yl)pentanoate (4). Compound **11** (209 mg, 0.48 mmol), compound **12** (259 mg, 0.53 mmol) and Et_3N (0.1 ml, 0.73 mmol) were dissolved in DMSO (2 mL), and stirred at 25 ^oC for 8 h. The mixture was extracted with CH_2Cl_2 and H_2O. The organic phase was dried over $MgSO_4$, filtered, concentrated under reduced pressure, and purified by flash chromatography on a silica gel column with elution of MeOH/CH_2Cl_2 (1:9) to give compound **4** (132 mg, 40%). The purity of product **4** was >99% as shown by HPLC on DIKMA column (Agilent, 4.6 × 250 mm, 5 μm), t_R = 19.9 min by elution with MeOH/EtOH (5:95) at a flow rate of 1.5 mL/min for 100 min. $C_{29}H_{40}N_8O_7S_2$; yellow foaming solid; $[\alpha]^{25}_D$ = +0.018 (*c* = 0.1, MeOH); IR ν_{max} (neat) 2392, 2923, 2871, 2360, 2341, 2110, 1698, 1648, 1599, 1466, 1333, 1285, 1238, 1203, 1115, 859, 762 cm^{-1}; ^1H NMR (400 MHz, $CDCl_3$) δ 7.98 (1 H, d, *J* = 8.4 Hz), 7.15 (1 H, d, *J* = 2.0 Hz), 7.03 (1 H, dd, *J* = 8.4, 1.2 Hz), 5.35 (1 H, s), 4.97 (1 H, s), 4.68 (2 H, s), 4.49−4.46 (1 H, m), 4.30−4.27 (2 H, m), 4.22–4.21 (1 H, m), 3.68−3.61 (13 H, m), 3.14−3.13 (1 H, m), 2.91−2.87 (1 H, m), 2.73−2.58 (6 H, m), 2.37 (2 H, t, *J* = 7.2 Hz), 1.68−1.64 (4 H, m), 1.43 (2 H, m); ^{13}C NMR (100 MHz, $CDCl_3$) δ 173.5, 165.0, 164.6, 163.6, 144.4, 143.3, 127.9, 120.2, 117.0, 109.9, 70.4, 70.2, 69.0, 68.6, 63.2, 61.8, 60.0, 57.4, 55.4, 53.2, 52.8, 44.9, 44.6, 41.9, 40.4, 33.7, 28.2, 28.1, 24.6; ESI−HRMS calcd for $C_{29}H_{41}N_8O_7S_2$: 677.2540, found: *m/z* 677.2524 $[M + H]^+$.

ASSOCIATED CONTENT

Supporting Information

Supplemental tables, figures, NMR spectra and HPLC diagrams. This material is available free of charge via the Internet at http://pubs.acs.org.

AUTHOR INFORMATION

Corresponding Authors

J.-M.F.: phone, 8862-33661663; fax, 8862-23637812; E-mail, jmfang@ntu.edu.tw.

S.-Y.S.: phone, 8862-28267233; E-mail: sysheu@ym.edu.tw

Notes

The authors declare no competing financial interest.

ACKNOWLEDGMENTS

We thank Mr. Guo-Chian Li at the Department of Chemistry, National Taiwan University, for his contribution to LC-MS/MS analysis. We are grateful to the Ministry of Science & Technology in Taiwan and Academia Sinica for financial support.

ABBREVIATIONS USED

Boc, *tert*-butoxycarbonyl; DMEDA, *N*,*N*′-dimethylethylenediamine; DTNB, 5,5′-dithiobis(2-nitrobenzoic acid); DTT, dithiothreitol; EDTA, ethylenediaminetetraacetic acid; HRP, horseradish peroxidase; GST, glutathione *S*-transferase; hTMPK, human thymidylate kinase; ITC, isothermal titration calorimetry; LID, ligand-induced degradation; MD, molecular dynamics; MM/PBSA, molecular mechanics/Poisson–Boltzmann Surface Area method; WST-1, 4-[3-(4-iodophenyl)-2-(4-nitrophenyl)-2*H*-5-tetrazolio]-1,3-benzene disulfonate; NADH, nicotinamide adenine dinucleotide; OD, optical density; PAINS, pan assay interference; PBS, phosphate-buffered saline; PEI, polyethyleneimine; P-loop, phosphate binding loop; PMA, phosphomolybdic acid; PME; Particle Mesh Ewald; PMSF, phenylmethylsulfonyl fluoride; PVDF, polyvinylidene difluoride; RMSD, root-mean-square deviation; RPMI medium, Roswell Park Memorial Institute medium; SDS–PAGE, sodium dodecyl sulfate polyacrylamide gel electrophoresis; TFA, trifluoroacetic acid; THF, tetrahydrofuran; TMPKmt, TMPK of *Mycobacterium tuberculosis*; TK1, thymidine kinase 1; Tris, tris(hydroxymethyl)aminomethane

REFERENCES

(1) Mathews, C. K. DNA synthesis as a therapeutic target: the first 65 years. *FASEB J.* **2012**, 26, 2231–2237.

(2) Hu, C. M.; Yeh, M. T.; Tsao, N.; Chen, C. W.; Gao, Q. Z.; Chang, C. Y.; Lee, M. H.; Fang, J. M.; Sheu, S. Y.; Lin, C. J.; Tseng, M. C.; Chen, Y. J.; Chang, Z. F. Tumor cells require thymidylate kinase to prevent dUTP incorporation during DNA repair. *Cancer Cell* **2012**, 22, 36–50.

(3) Liu, Y.; Marks, K.; Cowley, G. S.; Carretero, J.; Liu, Q.; Nieland, T. J.; Xu, C.; Cohoon, T. J.; Gao, P.; Zhang, Y.; Chen, Z.; Altabef, A. B.; Tchaicha, J. H.; Wang, X.; Choe, S.; Driggers, E. M.; Zhang, J.; Bailey, S. T.; Sharpless, N. E.; Hayes, D. N.; Patel, N. M.; Janne, P. A.; Bardeesy, N.; Engelman, J. A.; Manning, B. D.; Shaw, R. J.; Asara, J. M.; Scully, R.; Kimmelman, A.; Byers, L. A.; Gibbons, D. L.; Wistuba, II; Heymach, J. V.; Kwiatkowski, D. J.; Kim, W. Y.; Kung, A. L.; Gray, N. S.; Root, D. E.; Cantley, L. C.; Wong, K. K. Metabolic and functional genomic studies identify deoxythymidylate kinase as a target in LKB1-mutant lung cancer. *Cancer Discov.* **2013**, 3, 870–879.

(4) Ostermann, N.; Lavie, A.; Padiyar, S.; Brundiers, R.; Veit, T.; Reinstein, J.; Goody, R. S.; Konrad, M.; Schlichting, I. Potentiating AZT activation: structures of wild-type and mutant human thymidylate kinase suggest reasons for the mutants' improved kinetics with the HIV prodrug metabolite AZTMP. *J. Mol. Biol.* **2000**, 304, 43–53.

(5) Reynes, J. P.; Tiraby, M.; Baron, M.; Drocourt, D.; Tiraby, G. Escherichia coli thymidylate kinase: molecular cloning, nucleotide sequence, and genetic organization of the corresponding tmk locus. *J. Bacteriol.* **1996**, 178, 2804–2812.

(6) Lavie, A.; Vetter, I. R.; Konrad, M.; Goody, R. S.; Reinstein, J.; Schlichting, I. Structure of thymidylate kinase reveals the cause behind the limiting step in AZT activation. *Nat. Struct. Biol.* **1997**, 4, 601–604.

(7) Lavie, A.; Ostermann, N.; Brundiers, R.; Goody, R. S.; Reinstein, J.; Konrad, M.; Schlichting, I. Structural basis for efficient phosphorylation of 3'-azidothymidine monophosphate by *Escherichia coli* thymidylate kinase. *Proc. Natl. Acad. Sci. U. S. A.* **1998**, 95, 14045–14050.

(8) Ostermann, N.; Schlichting, I.; Brundiers, R.; Konrad, M.; Reinstein, J.; Veit, T.; Goody, R. S.; Lavie, A. Insights into the phosphoryltransfer mechanism of human thymidylate kinase gained from crystal structures of enzyme complexes along the reaction coordinate. *Structure* **2000**, *8*, 629–642.

(9) Whittingham, J. L.; Carrero-Lerida, J.; Brannigan, J. A.; Ruiz-Perez, L. M.; Silva, A. P.; Fogg, M. J.; Wilkinson, A. J.; Gilbert, I. H.; Wilson, K. S.; Gonzalez-Pacanowska, D. Structural basis for the efficient phosphorylation of AZT-MP (3'-azido-3'-deoxythymidine monophosphate) and dGMP by *Plasmodium falciparum* type I thymidylate kinase. *Biochem. J.* **2010**, *428*, 499–509.

(10) Kumar, M.; Sharma, S.; Srinivasan, A.; Singh, T. P.; Kaur, P. Structure-based in-silico rational design of a selective peptide inhibitor for thymidine monophosphate kinase of mycobacterium tuberculosis. *J. Mol. Model* **2011**, *17*, 1173–1182.

(11) Gardberg, A.; Shuvalova, L.; Monnerjahn, C.; Konrad, M.; Lavie, A. Structural basis for the dual thymidine and thymidylate kinase activity of herpes thymidine kinases. *Structure* **2003**, *11*, 1265–1277.

(12) Su, J. Y.; Sclafani, R. A. Molecular cloning and expression of the human deoxythymidylate kinase gene in yeast. *Nucleic Acids Res.* **1991**, *19*, 823–827.

(13) Cui, Q.; Shin, W. S.; Luo, Y.; Tian, J.; Cui, H.; Yin, D. Thymidylate kinase: an old topic brings new perspectives. *Curr. Med. Chem.* **2013**, *20*, 1286–1305.

(14) Sitkoff, D.; Sharp, K. A.; Honig, B. Accurate calculation of hydration free energies using macroscopic solvent models. *J. Phys. Chem.* **1994**, *98*, 1978–1988.

(15) Trott, O.; Olson, A. J. AutoDock Vina: improving the speed and accuracy of docking with a new scoring function, efficient optimization, and multithreading. *J. Comput. Chem.* **2010**, *31*, 455–461.

(16) Dorman, G.; Prestwich, G. D. Using photolabile ligands in drug discovery and development. *Trends Biotechnol.* **2000**, *18*, 64–77.

(17) Sumranjit, J.; Chung, S. J. Recent advances in target characterization and identification by photoaffinity probes. *Molecules* **2013**, *18*, 10425–10451.

(18) Tanaka, Y.; Bond, M. R.; Kohler, J. J. Photocrosslinkers illuminate interactions in living cells. *Mol. Biosyst.* **2008**, *4*, 473–480.

(19) Li, G.; Liu, Y.; Yu, X.; Li, X. Multivalent photoaffinity probe for labeling small molecule binding proteins. *Bioconjug. Chem.* **2014**, *25*, 1172–1180.

(20) Taldone, T.; Patel, P. D.; Patel, H. J.; Chiosis, G. About the reaction of aryl fluorides with sodium sulfide: investigation into the selectivity of substitution of fluorobenzonitriles to yield mercaptobenzonitriles via SNAr displacement of fluorine. *Tetrahedron Lett.* **2012**, *53*, 2548–2551.

(21) Andersen, J.; Madsen, U.; Bjorkling, F.; Liang, X. F. Rapid synthesis of aryl azides from aryl halides under mild conditions. *Synlett* **2005**, 2209–2213.

(22) Markiewicz, J. T.; Wiest, O.; Helquist, P. Synthesis of primary aryl amines through a copper-assisted aromatic substitution reaction with sodium azide. *J. Org. Chem.* **2010**, *75*, 4887–4890.

(23) Hajipour, A. R.; Mohammadsaleh, F. Preparation of aryl azides from aromatic amines in *N*-methyl-2-pyrrolidonium bisulfate. *Org. Prep. Proc. Int.* **2011**, *43*, 451–455.

(24) Li, Y.; Chase, A. R.; Slivka, P. F.; Baggett, C. T.; Zhao, T. X.; Yin, H. Design, synthesis, and evaluation of biotinylated opioid derivatives as novel probes to study opioid pharmacology. *Bioconjug. Chem.* **2008**, *19*, 2585–2589.

(25) Hu, C. M.; Chang, Z. F. A bioluminescent method for measuring thymidylate kinase activity suitable for high-throughput screening of inhibitor. *Anal. Biochem.* **2010**, *398*, 269–271.

(26) Sattler, M., Griffin, J. D.. Mechanisms of transformation by the BCR/ABL oncogene. *Int. J. Hematol.* **2001**, 73, 278–291.

(27) Vaidya, A. S.; Karumudi, B.; Mendonca, E.; Madriaga, A.; Abdelkarim, H.; van Breemen, R. B.; Petukhov, P. A. Design, synthesis, modeling, biological evaluation and photoaffinity labeling studies of novel series of photoreactive benzamide probes for histone deacetylase 2. *Bioorg. Med. Chem. Lett.* **2012**, *22*, 5025–5030.

(28) Baell, J. B.; Holloway, G. A. New substructure filters for removal of pan assay interference compounds (PAINS) from screening libraries and for their exclusion in bioassays. *J. Med. Chem.* **2010**, *53*, 2719–2740.

(29) Baell, J.; Walters, M. A. Chemistry: Chemical con artists foil drug discovery. *Nature* **2014**, *513*, 481–483.

(30) Phillips, J. C.; Braun, R.; Wang, W.; Gumbart, J.; Tajkhorshid, E.; Villa, E.; Chipot, C.; Skeel, R. D.; Kale, L.; Schulten, K. Scalable molecular dynamics with NAMD. *J. Comput. Chem.* **2005**, *26*, 1781–1802.

(31) MacKerell, A. D.; Bashford, D.; Bellott, M.; Dunbrack, R. L.; Evanseck, J. D.; Field, M. J.; Fischer, S.; Gao, J.; Guo, H.; Ha, S.; Joseph-McCarthy, D.; Kuchnir, L.; Kuczera, K.;

Lau, F. T. K.; Mattos, C.; Michnick, S.; Ngo, T.; Nguyen, D. T.; Prodhom, B.; Reiher, W. E.; Roux, B.; Schlenkrich, M.; Smith, J. C.; Stote, R.; Straub, J.; Watanabe, M.; Wiorkiewicz-Kuczera, J.; Yin, D.; Karplus, M. All-atom empirical potential for molecular modeling and dynamics studies of proteins. *J. Phys. Chem. B* **1998**, *102*, 3586–3616.

(32) Frisch, M. J.; Trucks, G. W.; Schlegel, H. B.; Scuseria, G. E.; Robb, M. A.; Cheeseman, J. R.; Scalmani, G.; Barone, V.; Mennucci, B.; Petersson, G. A.; Nakatsuji, H.; Caricato, M.; Li, X.; Hratchian, H. P.; Izmaylov, A. F.; Bloino, J.; Zheng, G.; Sonnenberg, J. L.; Hada, M.; Ehara, M.; Toyota, K.; Fukuda, R.; Hasegawa, J.; Ishida, M.; Nakajima, T.; Honda, Y.; Kitao, O.; Nakai, H.; Vreven, T.; Montgomery, Jr. J. A.; Peralta, J. E.; Ogliaro, F.; Bearpark, M.; Heyd, J. J.; Brothers, E.; Kudin, K. N.; Staroverov, V. N.; Kobayashi, R.; Normand, J.; Raghavachari, K.; Rendell, A.; Burant, J. C.; Iyengar, S. S.; Tomasi, J.; Cossi, M.; Rega, N.; Millam, J. M.; Klene, M.; Knox, J. E.; Cross, J. B.; Bakken, V.; Adamo, C.; Jaramillo, J.; Gomperts, R.; Stratmann, R. E.; Yazyev, O.; Austin, A. J.; Cammi, R.; Pomelli, C.; Ochterski, J. W.; Martin, R. L.; Morokuma, K.; Zakrzewski, V. G.; Voth, G. A.; Salvador, P.; Dannenberg, J. J.; Dapprich, S.; Daniels, A. D.; Farkas, Ö .; Foresman, J. B.; Ortiz, J. V.; Cioslowski, J.; and Fox, D. J. Gaussian 09, Revision E.01, Gaussian, Inc., Wallingford CT, 2009.

(33) Jorgensen, W. L.; Chandrasekhar, J.; Madura, J. D.; Impey, R. W.; Klein, M. L. Comparison of simple potential functions for simulating liquid water. *J. Chem. Phys.* **1983**, *79*, 926–935.

(34) Darden, T.; York, D.; Pedersen, L. Particle mesh Ewald: An *N*•Log(*N*) method for Ewald sums in large systems. *J. Chem. Phys.* **1993**, *98*, 10089–10092.

(35) Humphrey, W.; Dalke, A.; Schulten, K. VMD: visual molecular dynamics. *J. Mol. Graph.* **1996**, *14*, 33–8, 27–8.

(36) Kollman, P. A.; Massova, I.; Reyes, C.; Kuhn, B.; Huo, S. H.; Chong, L.; Lee, M.; Lee, T.; Duan, Y.; Wang, W.; Donini, O.; Cieplak, P.; Srinivasan, J.; Case, D. A.; Cheatham, T. E. Calculating structures and free energies of complex molecules: combining molecular mechanics and continuum models. *Acc. Chem. Res.* **2000**, *33*, 889–897.

(37) Ostermann, N.; Segura-Pena, D.; Meier, C.; Veit, T.; Monnerjahn, C.; Konrad, M.; Lavie, A. Structures of human thymidylate kinase in complex with prodrugs: implications for the structure-based design of novel compounds. *Biochemistry* **2003**, *42*, 2568–2577.

(38) Ngamwongsatit, P.; Banada, P. P.; Panbangred, W.; Bhunia, A. K., WST-1-based cell cytotoxicity assay as a substitute for MTT-based assay for rapid detection of toxigenic Bacillus species using CHO cell line. *J. Microbiol. Methods* **2008**, 73, 211–215.

Legend of Chart, Schemes and Figures

Chart 1. Chemical structures of **1a**, arene-fused isothiazolone analogues **1b**–**3b**, and photoaffinity probe **4**.

Scheme 1. Synthesis of hTMPK inhibitors **1b**–**3b**.

Scheme 2. Synthesis of probe **4**.

Figure 1. Structural model of hTMPK.

Figure 2. Binding modes of hTMPK–ligand complexes and the assay results.

Figure 3. Isothermal titration calorimetry (ITC) experiment.

Figure 4. Photoaffinity probe labeling.

Table of Contents (Graphic)